Study of 3D printed piezoresistive sensors for smart insole applications

Vereniki T. Mari
ph5046

Diploma Thesis

Supervisors

Dr. Alexandros Pantazis

Prof. Iliopoulos Eleutherios

University of Crete

Institute of Electronic Structure and Laser

Microelectronics Research Group (MRG)-Faculty of Applied Physics

Department of Physics

Heraklion, Crete

October 2022

Acknowledgements

First, I would like to express my gratitude to my supervisor Dr. Pantazis Alexandros, for his academic guidance throughout this study. Thank you for offering me a chance to be a part of this team and especially for your support during our collaboration.

On this note, I would like to acknowledge the assistance of Mr. Makris Georgios and Mr. Samarentsis Anastasios in helping me adapt in the laboratory and offering their insight and help throughout the experimentation process. A special mention to Mr. Makris is in order since the gait simulator set up used in the experimentation process of this study is his creation and to Mr.Giorgos Christodoulakis who created the program used visualize the changes of the pressure applied on the sensors in real time testing.

Furthermore, I would like to thank the members of the examination committee Prof. Iliopoulos Eleutherios and Dr. Aperathitis Elias not only for their interest in this work but also for their time and patience.

Last but not least I would like to thank my family and friends for inspiring me and being by my side throughout the process of completing this thesis.

This work was part of the Smart Insole (ΤΙΕΔΚ – 01888) research program.

Abstract

Gait analysis, or the study of human and animal locomotion has been the object of various studies for hundreds of years. Since the first proposal for a scientific description of gait analysis by Galileo in 1680, gait analysis has been used in medicine to study not only the physics of the human body movement but to also pinpoint potential pathological reasons altering the gait and stance. Advancements in technology including wearable sensors and podographs offer a detailed and precise analysis of each subphase of the gait cycle and thus provide diagnosticians with more precise and accurate results faster

Additive manufacturing is the process of creating a three-dimensional structure by adding layers of material instead of subtracting. 3D printing, aided by specialized software, allows the user to create intricate and precise designs at a low cost and fast rate, in a controlled environment. Additive manufacturing, with recent advances in technology that made the creation of flexible, conductive and even biocompatible filaments possible has become a valuable tool in a variety of fields, from engineering to medicine.

In this study, the goal is to develop a set of 3D printed piezoresistive sensors for further applications in entirely 3d printed smart insoles. The study itself, consists of not only designing, but also testing the piezoresistive properties and the sensitivity to environmental changes of three flexible conductive filaments.

In the first part of the thesis, a brief history of gait analysis and additive manufacturing is presented, along with their importance in developing wearable sensors and specifically smart insoles for diagnostic applications.

The printers and filaments utilized in this experiment, along with the geometric characteristics of the sensors, are described in *Section 2: Materials and Methods.* Furthermore, a detailed description of the gait simulator set-up and the process of calibrating the set up and preparing the samples for testing is described in detail. In the last part of the section, the data collection process along with explanatory figures is presented.

The Data collection section, contains the collective tables containing data for both the original and the measurements related to testing the aging of the samples

The 4th part of this study is dedicated to data analysis. First, the formulas used to transform the weight applied and the resistance value units to pressure and Ohm respectively are presented. The data analysis process is described, along with the resulting figures which illustrate the results for how the resistance of each sample changes with different amounts of pressure applied. In order to conclude which sample has the highest sensitivity the graphs were fitted using tools provided by *Origin*. The process of reaching a conclusion concerning the optimal sensor is described in detail and accompanied by the formulas utilized. Lastly, figures showcasing how the resistance of each sample changes when exposed to different humidity percentages and temperatures as time passes accompanied by the conclusion that derives from figure comparison is presented.

In the two final sections, the collective results indicating both the sensitivity of the sensors to pressure changes and environmental factors are compared and discussed in order to reach a conclusion as to which filament and sensor design is optimal and could potentially be utilized in smart insole applications. Furthermore, a review of the whole experimentation and analysis process, including difficulties and figures showcasing errors presented in the duration of the experiment is given along with the results of real time experimentation with the sensors placed inside a 3D printed insole. Eventually, the conclusion that derives from this study is that 3D printed piezoresistive sensors seem to be unsuitable for smart insole applications due to both their sensitivity to changes in humidity and temperature but also due to the instability in the resistance of each sample even in a relaxed state since the differentiation of which resistance changes occur due to an alteration in the wearer's gait cycle and which are a result of sensor sensitivity compromission is almost impossible.

Finally, a list of references is included while in the appendix section the collective tables for the resistance values obtained during the data collection process for each sensor are presented.

Contents

Abbreviations

3D:	Three dimensional
ABS:	Acrylonitrile Butadiene Polystyrene
CAD:	Computer Aided Design
FBG:	Fiber Bragg Grating
FDM:	Fused Deposition Modeling
FEAM:	Fiber Encapsulation Additive Manufacturing
GCPM:	General Conference on Weights and Measures
HIBM:	Hereditary Inclusion Body Myopathy
SCARA:	Selective Compliance Robot Arm
SI:	System International.
SLA:	Stereolithography
SLS:	Selective Laser Sintering
TEAM:	Thermoplastic Elastomer Additive Manufacturing
UV:	Ultraviolet

Figure Index

Table Index

1. Introduction

1.1. Gait Analysis.

1.1.1. Human Gait Cycles

The gait cycle is typically assessed as the intermission between two consecutive contacts of the foot with the ground and is studied separately for each limb. Usually, the gait cycle can be divided into two phases, the stance and the swing which are further divided respectively into four and three sub-phases, according to the significance of the movements included in the cycle, the temporal and tractional qualities of the stride itself and the reciprocal foot changes. [(1)]

The first sub-phase of the stance is the heel strike (A) or initial contact with the ground where the reaction force from the ground that opposes the force of weight applied appears only at the heel. The loading response (B) that follows the heel strike describes the period of time between the initial contact with the ground and the lift of the opposite leg and is characterized by the shifting of the weight. The following simultaneous contact of the heel and forefoot with the ground signals the beginning of the mid-stance (C) phase, preceded by the terminal stance (D) during which the center of mass transits forward and the heel is no longer in contact with the ground. The terminal stance indicates the ending of the stance phase and if followed by the pre-swing (E), indicating the beginning of the swing phase and explained as the time period between the initial contact of the contralateral extremity to the beginning of the lift of the ipsilateral extremity from the ground. During this time the second shift of weight is observed. The initial and mid-swing (F) phase indicate exertion of the swinging limb which moves forward while the other is in the mid stance phase. In the terminal swing (G), the heel of the swinging limb is in contact with the ground and the gait cycle is completed as shown in the figure below. [(1) (2)]

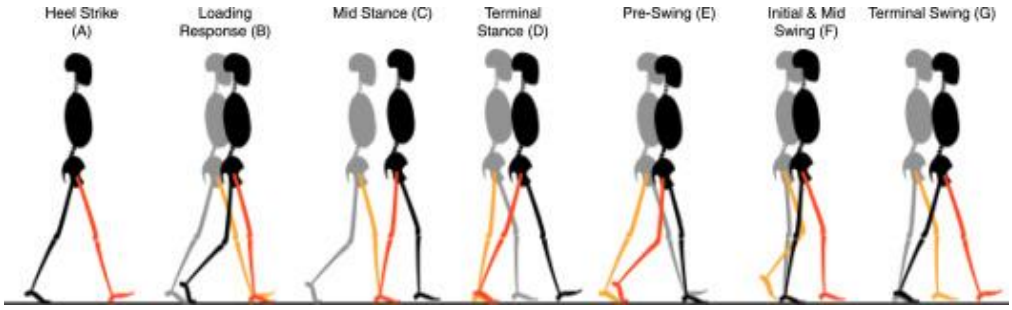

Figure 1.1.1: Gait Phases and Sub-Phases. [(1)]

1.1.2. What is Gait Analysis

The term gait analysis describes the study of animal or human locomotion. The first scientific method for locomotion analysis was introduced by Galileo and applied in 1680 by Borelli, although the value of that experiment is almost entirely historical since the lack of available monitoring tools of the subject resulted in a quasi-static approach of the experiment. With further technological advances in photography, the first images of animals and humans in motion were published by Muybridge in 1887 and since then, advances in technology and especially automatization have aided the three-dimensional observation of body movement.[(3)(5)]

In the field of medicine, measuring of cadence, the number of steps per minute, velocity of the body and stride length, characteristic parameters of a patient's gait cycle assist in pinpointing anomalies caused by neuromusculoskeletal dysfunction or a variety of pathological reasons, therefore, providing in a variety of cases the diagnosticians with insight into the causes of anomalies in the gait cycle of a patient. [(4)]

1.1.3. Advances in Gait Analysis

Gait analysis for many years was limited to visually observing the subject walking. Recent advances in technology have resulted in the use of accelerometers and wearable sensors that can give further insight into

the locomotive of a patient, offering more precise and detailed results as to the physics of overall movement. Advances in technology resulted in the development of podometry mats, podographs and wearable sensors in insoles specifically designed to analyze not only the gait cycle as a whole but each sub-phase of the cycle individually. Used to identify anomalies in the gait cycle and posture of patients, monitor the healing process after injuries, calculate athletic performance, and even assist in developing footwear.

A platform system for gait analysis such as Tekscan's Strideway, a mat that consists of sensor tiles and a corresponding software in order to visualize the user's gait cycle in real-time is used worldwide by podiatric specialists and researchers. The platform systems of gait observation require space to be set, and the sensory mat has limitations in its dimensions, therefore collecting objective data from consecutive steps or running is still a challenge.

Figure 1.1.2. : Tekscan's Strideway and Tekscan's F-Scan and F-Scan64. (6)

Developments in the field of wearable sensors have been made to overcome these challenges, offering a more objective view of a patient's gait cycle. Insoles, wireless or not, such as F-Scan and F-Scan64 systems by Tekscan prevent targeting, the alteration of the gait during the use of a podometry mat due to the lack of space, offers insight into the position of the foot inside the footwear and allows testing on different environments or paces. (Running, going up or down a set of stairs, etc.) [(6)]

1.2. Additive Manufacturing

1.2.1.A Brief History of Additive Manufacturing.

The first patent for additive manufacturing was issued in 1986 to Charles Hull, who a few years prior developed a method of creating three-dimensional structures by curing a photosensitive resin with ultraviolet radiation, a technique since known as Stereolithography (SLA). The earliest application of stereolithography though seem to have been in 1981 in Japan by Hideo Kodama, who was unable to credit the patent for himself. In 1988, the 3D Systems Corporation was founded by Hull, and the first commercial SLA printer (SLA-1) was released in the same year.

At the same year, Carl Deckard in the University of Texas developed another method of additive manufacturing similar to SLA, which instead of curing a photosensitive liquid resin, fused together powders using a laser. (Selective Laser Sintering SLS)

The third and most distinctive method of additive manufacturing, is FDM (Fused Deposition Modeling) or Fused Filament Fabrication which is a (trademarked by Stratasys in 1991) name for the same technique was created by Scott Crumb. The distinctive feature of this method is that instead of curing resins with radiation, the filament that will create the print is extruded directly from a heated nozzle.

With the rapid advances in technology since 1990, CAD tools became commonly available bringing the 3D design process closer to the public. In 2006 the first commercial SLS printer was released and in 2005, Dr.

Adrian Bowyer created the RepRap project, an initiative to create a 3D printer that could create itself, and in 2008, the first prosthetic leg was created.

Since 2009, when the patents for 3D printing became available to the public, printers and printing materials have become more accessible to the public and printing has become faster, safer and more precise, paving the way for more delicate applications of the technique in various fields. [7]

In total, there are 12 distinctive 3D printing methods. [8][15] Each method has its own advantages and disadvantages and the choice depends on the budget, time available, printing materials and complexity of the desirable structure of the print.

1.2.2.FDM Printing

In Fused Deposition Modeling the three-dimensional structure is created by extruding a heated filament through a nozzle layer-by-layer on the printer bed. The heated layers are fused together without the need for further curing, and the filament is heated past the glass melting point. [16]

The most common filaments used in FDM printing are thermoplastics but since 3d printing has become widely used in a variety of fields, the need for different kinds of filaments, has created materials with a variety of properties like conductivity, flexibility, higher endurance or aesthetic value, and even edible and biodegradable.[17][18]

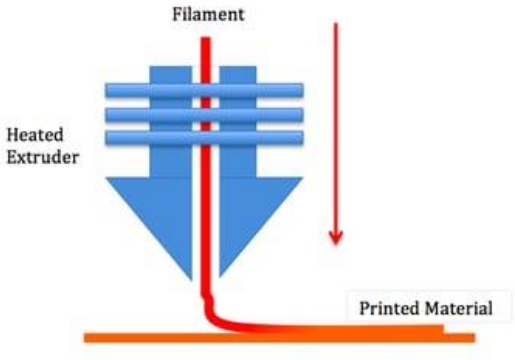

Figure 1.2.1: FDM printing process. [16]

FDM Printers can be derived in two major categories. In Cartesian FDM Printers, the extruders move linearly along the x,y,z- axis, and use the Cartesian system in order to coordinate the placement of the print and to calibrate the extruders. In the case of polar FDM printers, first issued in 2015, angle and distance instead of x and y-axis is used in order to calibrate the placement of the print along with a circular instead of a rectangular grid. The extruder moves through the z-axis as layers are added on the print.

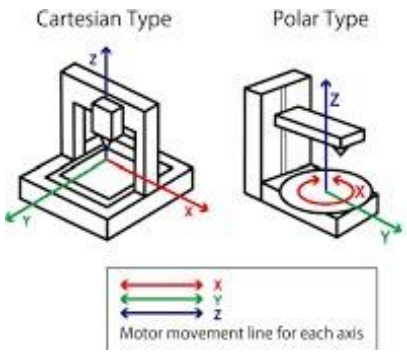

Figure 1.2.2: Differences in the coordination system of Cartesian and Polar Type 3D printers. [17]

Cartesian Printers can be divided in three sub categories. In the first, Rectilinear, or traditional Cartesian printers the extruders move in fixed x,y,z axis.

In the second category, Delta 3D printers, the extruder is not attached to fixed axes but in three or more mechanical arms that are attached to a vertical rail and together calibrate the position of the nozzle relatively to the printer bed.

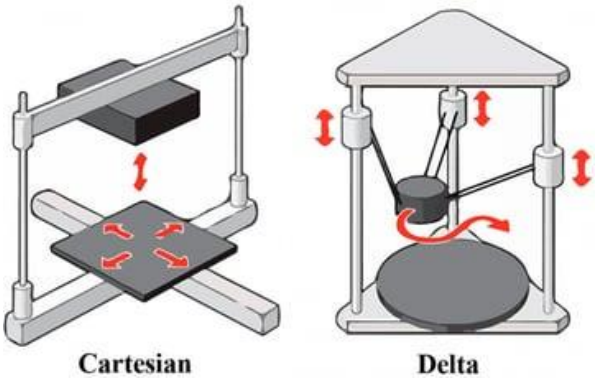

Figure 1.2.3: Differences between Cartesian and Delta FDM printer. [18]

The third category, Selective Compliance Assembly Robot Arm (SCARA) or Robotic Arm printers in general, is still in a developmental state. This printing process does not require a printing plate (bed) and the extruder is attached to a robotic arm allowing much more flexibility in movement and therefore can result in more complex prints in less time, though it seems to negatively affect the final print quality. [14]

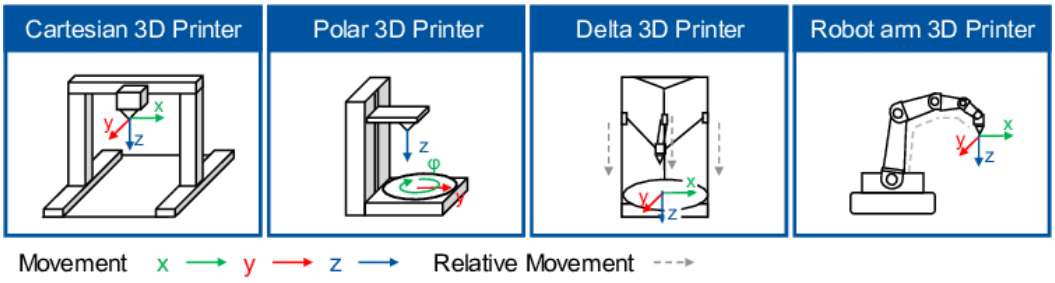

Figure 1.2.4: Differences in extruder movement and coordination systems of the four FDM printer types.[14]

1.3. Piezoresistive Effect

1.3.1. What is the Piezoresistive Effect

The piezoresistive effect describes a change in the electrical resistivity of a conductive material due to the application of mechanical strain. The electric potential in the case of piezoresistive effect remains unchanged. The piezoresistive effect was first observed in 1856 by Lord Kelvin and with the developments of digital circuits and vast use of semiconductor, in 1956 the large piezoresistive effect in silicon and germanium was observed. [19][20]

1.3.2. General Mechanism of the Piezoresistive Effect

The strain applied in conductors and semiconductors, induces changes in the spacing of the bandgaps (energy gaps) resulting in easier raise of electrons to the conduction band (ionization) and therefore changes the conductivity or resistivity of the materials. When the strain applied is between certain values thus resulting in a linear relationship between the pressure applied and the intensity of the ionization, the piezoresistive coefficient is constant.

$$\rho_\sigma = \frac{\left(\frac{\partial \rho}{\rho}\right)}{\varepsilon} \tag{1.3.1}$$

$$\varepsilon = \frac{\Delta L}{L} \tag{1.3.2}$$

Where ρ_σ is the piezoresistive coefficient, ε is the strain, which can be defined as the relative change in length as shown in *Equation 1.3.2* and ρ is the original resistivity of the material.

1.3.3. Piezoresistive Pressure Sensors

Piezoresistive pressure sensors, depending on the material they are created of are characterized by high sensitivity and linearity. With applications in various fields, pressure sensors, were one of the first pressure measurement devices to be commonly released and are one of the simplest piezoresistive devices. [22] [24]

A piezoresistive sensor, utilizes a conductive strain meter that alters its electrical resistance when strain is applied, and can be attached to a diaphragm that converts the change in resistance that occurs when the sensor is deformed in an electric signal.

Changes in a conductor's resistance result usually due to alterations in the conductor's dimensions, since the resistance of a conductor is proportional to its length, according to Ohm's law:

$$R = \frac{L}{A}\rho \tag{1.3.3}$$

Where R is the resistance of the conductor, L the length, ρ the original resistivity and A the area through which the current passes. At the same time, according to Ohm's law the cross-sectional area A is inversely proportional to the resistance, therefore a decrease of A signifies an increase in resistance. Furthermore, in certain materials the inherent resistivity increases when the material is stretched.

1.4. 3D Printed Pressure Sensors

As mentioned previously, recent developments in the process of 3D printing result in the utilization of conductive filaments, thus paving the way in creating complex electronic parts and high-functioning sensors in less time, for a reduced cost and with the ability to combine materials.[22][25]

Specifically in the case of pressure sensors that require multiple micro electromechanical systems (MEMS) the utilization of additive manufacturing may result in optimization of existing features without the high current costs.[21][25][26] Laszczaket al.[25][26] , introduced a 3D printed capacitance-based sensor, for lower-limb amputees in order to monitor the strain in the stump-socket region. The utilization of 3D printed resulted in low manufacturing costs, with a final product not only designed specifically for the limb residua of the wearer, but with maintaining the linearity when pressure or sheer strain was applied. (5-8%, for 1.3KPa and 0.6kPa respectively). Another capacitive force sensor was created by Saari et all, [25][27] who combined fiber encapsulation additive manufacturing (FEAM) and thermoplastic elastomer additive manufacturing (TEAM). The drawback, according to the test results seems to be an 8.3s delay appearing in the capacitance measurement during unloading for which the material hysteresis seems to be responsible. Another notable application is the design and fabrication of an ear prosthesis using polyvinylidene fluoride (PVDF) by Suaste-Gómez, proven to be functioning under a maximum pressure of 16,350Pa and a maximum temperature of 90°C[25][28], while Lin et all enabled Fiber Bragg grating (FBG),in a 3D-printed acrylonitrile butadiene styrene (ABS) body and proved the linear correlation between the FBG wavelength and the amount of pressure applied while the sensor itself showed a sensitivity of 0.208nm/bar.[25][29]

Piezoresistive sensors casted in a square mold with a photopolymer and then photocured with UV light with screen printed electrodes embedded in 3D printed tires, as proposed by Md Omar Faruk Emon and Jae-Won Choi, appear to be able to detect not only the amount of pressure or strain applied in them but also their directions. [25][30]

It is concluded that in regard to sensors, the utilization of additive manufacturing could improve existing technologies, while paving the way for the creation of sensors with improved durability and sensing properties

while maintaining a low cost of manufacturing, reducing the time needed to create each sensor and providing the developer with the ability to customize the sensor's geometrical and mechanical factors. As stated previously, the improvements in existing methods and the development of new technologies have only begun and paving the way for the introduction of a new generation of materials and tools.

2. Materials and Methods

2.1. Printing

2.1.1.Printing Materials

For the prints, four different conductive filaments, whose properties are shown in *Table 2.1.1* were used. To print the main bodies of the sensors we used **Ninjatek EEL**[33],**PI-ETPU 95-250 Carbon Black**[34]and **Filaflex Conductive**[35]which all have flexible properties and in order to print the top and middle layers in the case of the dual filament samples, **Protopasta Conductive PLA.**[36]The printing speed advised by the manufacturer in all case is 20mm/sec.

Material	Manufacturer	Printing Temp.	Hardness	Bed Temp	Vol. Resistivity	Type	Density
PI-ETPU	*Palmiga Innovation*	$210-230$ ℃	$95A\ Shore$	*N/A*	$\sim 800\Omega \cdot Cm$	TPU	$1.3 g/cm^3$
Eel	*Ninjatek*	$220-230$ ℃	$90A\ Shore$	$20-45$ ℃	$1.5 \cdot 10^3 \Omega \cdot cm$	TPU	$1.2 g/cm^3$
Filafelx Conductive	*Recreus*	$245-250$℃	$92A\ Shore$	$50-60$ ℃	$3.9\ \Omega \cdot cm$	TPU	$1.35 g/cm^3$
Protopasta Conductive	*ProtoPlant*	215 – 230℃	N/A	~50℃	$15\ \Omega \cdot cm$	PLA	$1.15 g/cm^3$

Table 2.1.1: Filament Characteristics. The volume resistivity refers to the resistivity of the filament in the raw material form and does not indicate the resistance of the printed sensor.[33][34][35][36]

2.1.2.Printers

The two printers and slicing software that were used afor the manufacturing of the sensors are the one-extruder **Original Prusa i3 MK3S+**[37]with the corresponding slicing software (**Prusa Slicer**) and the dual-extruder **Tenlog DMP 3D printer**[38] with **Ultimaker Cura**[39] as the preferred slicing software.

Figure 2.1.1.: Tenlog DMP 3D printer and Original Prusa i3 MK3S+[38][37]

2.1.3.Design

In the following table (*Table:2.1.2*) the dimensions of the sensors are shown. The sensors were designed with **Autodesk Fusion 360**[32] (student edition) and the final print is shown in *Figure 2.1.1.* The specific dimensions were set in order for an optimal number of sensors to fit comfortably inside a 3D printed insole.

Shape	Height (mm)	Diameter (mm)
Cylinder	3	14.5

Table 2.1.2: Sensor Dimensions

Even though the geometric factors (shape, height and diameter) of the prints were kept intact, in total three different designs were used as shown in *Figure 2.1.3.*

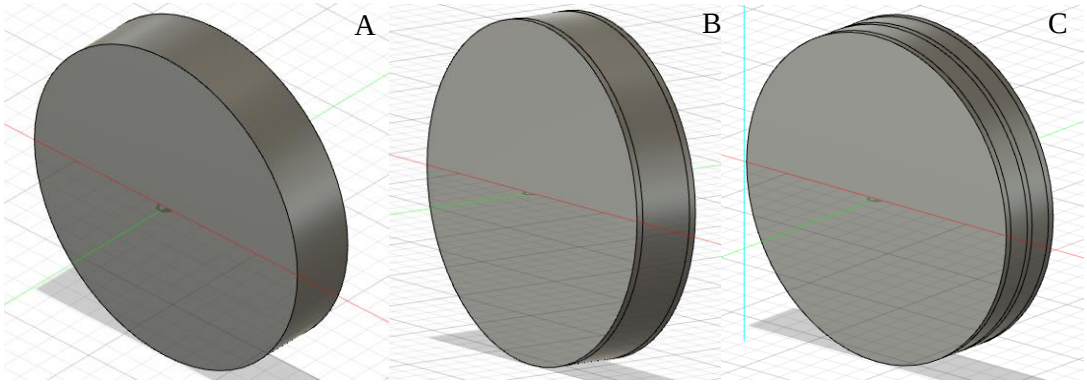

Figure 2.1.3: A) Single filament sensor design B) Sensor design with two protopasta layers C) Sensor design with three protopasta layers.

The first, as shown in *Figure 2.1.1*. results in a solid, cylindrical shape, printed with a single filament. This design was also used to create samples with different infill percentages of the same filament. The second design, included two layers of an inflexible conductive filament (*Protopasta* [36]*)* placed on top and bottom of the cylindrical shape. The total height of the sample did not change and each individual filament layer has a height of $0.3mm$. The third design is similar to the second one, but a third layer of Protopasta is added in the middle of the sensor.

Design Type	Description
$fil\_\%\_i$	Single filament sample. "%" indicates the infill percentage, fil the filamentand i the sample.
$proto\_fil\_i$	Sample with two protopasta layers (top/bottom). i indicates the sample and fil the filament
$middle\_fil\_i$	Sample with three protopasta layers (top/middle/bottom) i indicates the sample and fil the filament
fil_i	First print of a single filament sample. fil indicates the filament and i the sample.

Table 2.1.3: Code names and descriptions for the different designs used.

2.2. Dynamic Measurement Set-Up

2.2.1.Gait Simulator Set Up

In order to simulate the gait cycle and test the piezoresistive properties of each print, a dynamic measurement set-up was used. The gait simulator itself consists of a mechanical piston weighting 0.7kg, on which weights can adjusted. The set-up is powered by a generator operating at a voltage of $5.00 \pm 0.10V$ and Arduino microcontroller regulated the speed of the piston oscillation.

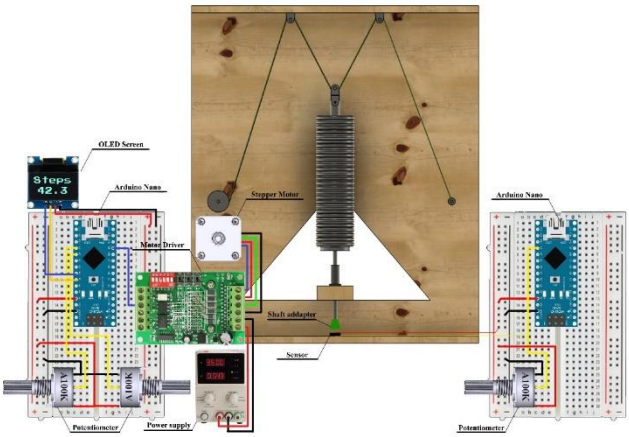

Figure 2.2.1: The gait simulator set-up which was used to test each sample's resistivity, and the corresponding control Arduino circuits.

For every measurement, the frequency was kept relatively constant at a pace of $40.00 \pm 0.01\ steps/min$ which when needed, could be adjusted by a potentiometer operating as an electrical dimmer. The total measurement time was kept at 2 minutes per weight value.

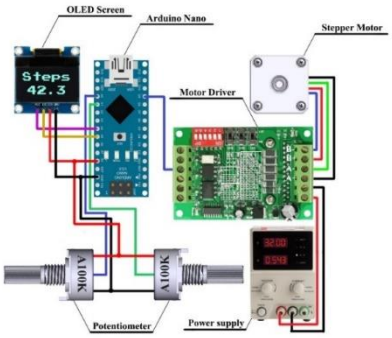

Figure 2.2.2: The control circuit for the gait simulator set up.

2.2.2.Placement of Sensors and Calibration

During the testing process, the sample was secured at the bottom of the set-up with non-conductive electrical tape, as shown in *Figure 2.2.1* so as the piston perfectly sits on top, in order to achieve an equal amount of pressure.

The sensor was connected to a second Arduino as shown in *Figure 2.2.2*, which collected data of the changes in the sample's resistance as the applied pressure changes during the gait simulation cycle. This circuit translated voltage passing through the sensor to a fixed value with a max of $1023 \pm 1 points$ corresponding to $5.00 \pm 0.01V$. In order to calibrate the system; before each measurement session, a potentiometer (10KΩ and 100KΩ max) connected to the Arduino UNO circuit was used. The max fixed value corresponds to the voltage when the maximum weight was placed on the setup and was fixed at $950 sens$.

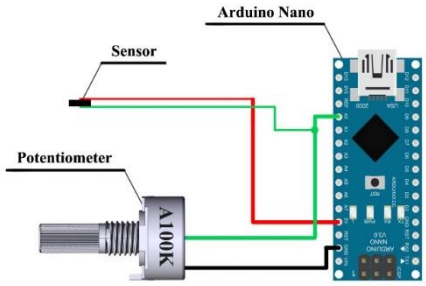

Figure 2.2.3: The circuit that records the changes in responsivity of the sample in the simulator during the gait cycle simulation. It should be noted here that the Arduino board that was finally used was Arduino UNO and not Arduino Nano as shown.

2.3. Data Collection

2.3.1.Purpose and Sections

The purpose of this study was to measure and compare 3D printed piezoresistive sensors fabricated with different materials. Since this research focused on the filaments that could be used in order to observe a change in the sensor resistance when pressure is applied without compromising on sensor durability, the geometrical factors were kept the same (*Table 2.1.1*) for each print.

The testing process was divided into two parts. In the first, for each design mentioned in *Table 2.1.2*, three samples were printed. Therefore, the resistivity of 42 samples in total was tested, in regard to the print infill, filament used and combination of inflexible and flexible conductive filaments.

The second part was dedicated to testing how time and environmental factors such as changes in humidity and temperature could wear the sensors and affect their sensitivity. Data was collected from each sample, for 5 times in total including the default first measurement, after periods of exposure to laboratory environment conditions while not in use. Specifically, the samples were stored for approximately two weeks after being tested. The exception is the case of the sensors with added protopasta layers and the first single filament print, were the first (default) test was done approximately 3 months before the first aging test.

2.3.2.Data collection process

After each measurement section the data collected are in the following form (*Table 2.3.1*) with the time values starting from 2 to 120000msec. The $Sens$ column corresponds to the sample's resistivity in fixed values which will be translated to S.I. resistance values. The $Volts$ column corresponds to the voltage that passes through the sensor during each measurement.

Time	Sens	Volts
2	676	3.11
4	676	3.11
6	677	3.11
8	676	3.11
10	675	3.10
12	675	3.10
14	675	3.10
16	677	3.11
18	677	3.11

Table 2.3.1: Indicative table of values obtained after one gait cycle.

From each measurement that corresponds to a certain weight, an average resistivity value was collected. In order to finalize the average value for each weight, the average of 10 consecutive maximum and 10 consecutive minimum peaks was calculated. The difference between each max and min along with the

average was calculated along with the standard deviation of these 10 values in each case. *Figure 2.3.1* and *Figure 2.3.2* are two indicative response diagrams for one of the samples (single filament eel sensor with 100% infill) for 0.7kg and 14.7kg, that showcase how the sample's resistance changes as the weight applied increases.

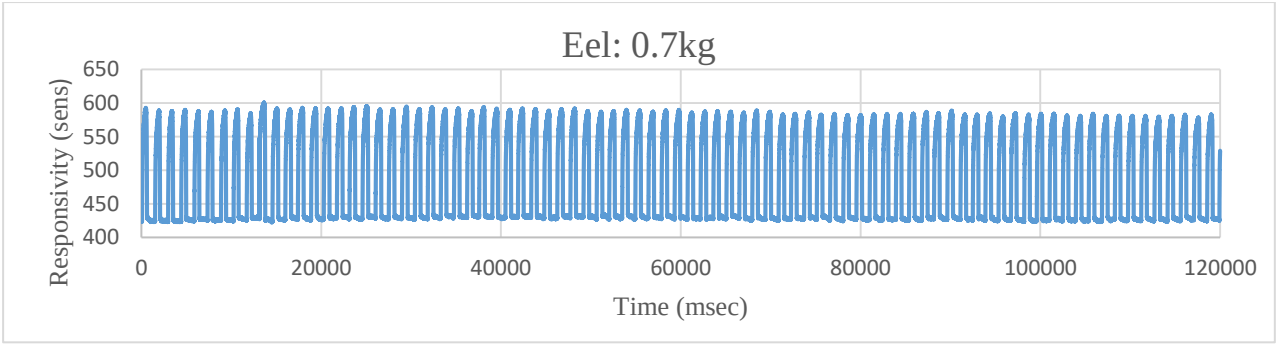

Figure 2.3.1: Indicative response diagram for single material eel sensor no1. for a total weight of 0.7Kg applied. 10 maximum and 10 minimum consecutive peaks were chosen from this diagram and their average was calculated.

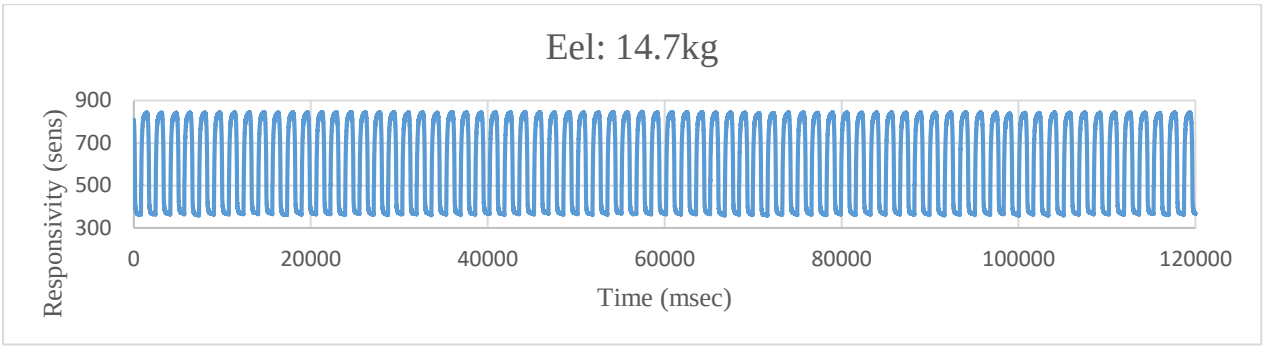

Figure 2.3.2: Indicative response diagram for single material eel sensor no1. for a total weight of 14.7Kg applied. 10 maximum and 10 minimum consecutive peaks were chosen from this diagram and their average was calculated.

The data collection and processing do not change drastically for the aging tests. Since the purpose is to observe the effect of environmental factors on the samples, each aging test was done with maximum weight was attached to the gait simulator with a total measurement time of 2 minutes. Before each measurement the Arduino max was set to 950sens as before and the corresponding potentiometer resistance was noted.

The data collection process has not changed, but since the maximum change in the sensor's resistance is observed when the maximum pressure is applied, data for each sensor were collected only for $14.7 \pm 0.01\ Kg$.

Furthermore, since the point of this set of tests was to indicate how and if environmental factors affect the samples, for every day that data was collected, the temperature and humidity percentage in the laboratory was noted before the data collection process begun.

3. Data Collection

3.1. Default Measurements

3.1.1.Ninjatek eel samples

In the following table, (*Table 3.1.1*) for each 3D printed sample, the corresponding potentiometer resistance values when the Arduino max value is fixed at $950 sens$ are shown.

Sensor	Potentiometer Resistance Value (KΩ)
eel_1	0.42 ± 0.01
eel_2	2.14 ± 0.01
eel_3	4.15 ± 0.01
proto_eel_1	1.03 ± 0.01
proto_eel_2	0.88 ± 0.01
proto_eel_3	0.97 ± 0.01
middle_eel_1	2.39 ± 0.01
middle_eel_2	3.98 ± 0.01
middle_eel_3	3.60 ± 0.01
eel_20_1	4.35 ± 0.01
eel_20_2	3.55 ± 0.01
eel_20_3	4.35 ± 0.01
eel_40_1	2.06 ± 0.01
eel_40_2	2.65 ± 0.01
eel_40_3	2.74 ± 0.01
eel_60_1	5.16 ± 0.01
eel_60_2	5.96 ± 0.01
eel_60_3	6.78 ± 0.01
eel_80_1	0.79 ± 0.01
eel_80_2	1.63 ± 0.01
eel_80_3	2.16 ± 0.01
eel_100_1	1.30 ± 0.01
eel_100_2	2.93 ± 0.01
eel_100_3	3.25 ± 0.01

Table 3.1.1: Potentiometer resistance values for 950sens for eel sensors

As previously mentioned, for each weight value, the average of 10 maximum and minimum peaks was calculated along with the corresponding standard deviation. In *Appendix A,* (*Tables A.1-A.24)* the collective average values for both the minimum and maximum peaks are shown.

3.1.2.Pi-ETU samples

Sensor	Potentiometer Resistance Value (KΩ)
pi_1	4.25 ± 0.01
pi_2	7.15 ± 0.01
pi_3	10.18 ± 0.01
proto_pi_1	6.73 ± 0.01
proto_pi_2	6.05 ± 0.01
proto_pi_3	8.43 ± 0.01
middle_pi_1	2.13 ± 0.01
middle_pi_2	1.97 ± 0.01
middle_pi_3	2.14 ± 0.01
pi_20_1	2.82 ± 0.01
pi _20_2	2.54 ± 0.01
pi _20_3	1.36 ± 0.01
pi _40_1	1.94 ± 0.01
pi _40_2	0.79 ± 0.01
pi _40_3	0.89 ± 0.01
pi _60_1	1.05 ± 0.01
pi _60_2	0.56 ± 0.01
pi _60_3	050 ± 0.01
pi _80_1	0.57 ± 0.01
pi _80_2	034 ± 0.01
pi _80_3	0.36 ± 0.01
pi _100_1	11.20 ± 0.01
pi _100_2	12.94 ± 0.01
pi _100_3	12.34 ± 0.01

Table 3.1.2: Potentiometer resistance values for 950sens for pi-etu sensors

3.1.3.Filaflex samples

Sensor	Potentiometer Resistance Value (KΩ)
fila_1	0.50 ± 0.01
fila _2	0.86 ± 0.01
fila _3	0.74 ± 0.01
proto_fila_1	1.71 ± 0.01
proto_fila_2	1.41 ± 0.01
proto_fila_3	2.41 ± 0.01
middle_fila_1	1.49 ± 0.01
middle_fila_2	1.52 ± 0.01
middle_fila_3	3.99 ± 0.01
fila_20_1	1.66 ± 0.01
fila _20_2	0.77 ± 0.01
fila _20_3	0.80 ± 0.01
fila _40_1	0.84 ± 0.01
fila _40_2	0.31 ± 0.01
fila _40_3	0.32 ± 0.01
fila _60_1	0.86 ± 0.01
fila _60_2	0.31 ± 0.01
fila _60_3	0.32 ± 0.01
fila _80_1	0.72 ± 0.01
fila _80_2	0.61 ± 0.01
fila _80_3	0.51 ± 0.01
fila _100_1	2.50 ± 0.01
fila _100_2	0.99 ± 0.01
fila _100_3	1.33 ± 0.01

Table 3.1.3: Potentiometer resistance values for 950sens for filaflex sensors.

3.2. Aging

3.2.1.Ninjatek eel samples.

Table 3.2.1, includes the corresponding potentiometer resistance values, when the Arduino max value is fixed at $950sens$ in regard with temperature and humidity percentage for each one of the 5 times that data was collected for each one of the eel samples. The collective average values for the 10 maximum peaks when maximum amount of pressure is applied and the corresponding error for each measurement are also shown.

Similarly, *Table 3.2.2.* and *Table 3.2.3.,* contain the corresponding information for pi-etu and filaflex samples.

Sample	Date	Potentiometer Resistance Value (KΩ)	Max Resistance Value (sens)	Error (sens)	Temperature	Humidity
eel_1	21/03	2.39 ± 0.01	890.40	2.46	22.0℃	29%
	05/04	2.43 ± 0.01	817.20	1.08	22.0℃	42%
	20/04	8.53 ± 0.01	933.40	2.73	19.3℃	50%
	03/05	2.10 ± 0.01	864.70	0.64	21.0℃	45%
proto_eel_1	21/03	1.05 ± 0.01	957.60	0.49	22.0℃	29%
	05/04	0.91 ± 0.01	948.00	0.00	22.0℃	42%
	20/04	1.02 ± 0.01	947.30	0.64	19.3℃	50%
	03/05	1.42 ± 0.01	948.30	0.46	21.0℃	45%
middle_eel_1	21/03	1.70 ± 0.01	947.60	0.49	22.0℃	29%
	05/04	1.23 ± 0.01	947.10	0.70	22.0℃	42%
	20/04	1.62 ± 0.01	947.80	0.87	19.3℃	50%
	03/05	1.35 ± 0.01	945.50	0.67	21.0℃	45%
eel _20_1	09/02	4.35 ± 0.01	940.90	1.76	21.4℃	37%
	01/03	6.38 ± 0.01	903.90	1.70	18.6℃	52%
	15/03	2.36 ± 0.01	873.60	1.80	21.5℃	31%
	29/03	11.25 ± 0.01	889.30	2.33	19.1℃	50%
	15/04	4.68 ± 0.01	877.30	2.97	18.5℃	40%
eel _40_1	09/02	2.06 ± 0.01	906.50	1.43	21.7℃	35%
	01/03	7.12 ± 0.01	901.40	2.37	18.6℃	52%
	15/03	0.94 ± 0.01	873.80	1.94	21.5℃	31%
	29/03	4.70 ± 0.01	853.80	2.68	19.1℃	50%
	15/04	9.32 ± 0.01	896.50	1.69	18.5℃	40%
eel _60_1	10/02	5.16 ± 0.01	931.90	1.45	19.8℃	47%
	01/03	5.30 ± 0.01	905.10	1.14	18.6℃	52%
	15/03	0.85 ± 0.01	880.20	1.33	21.5℃	31%
	29/03	1.34 ± 0.01	833.70	2.24	19.1℃	50%
	15/04	4.01 ± 0.01	898.20	1.40	18.5℃	40%
eel _80_1	10/02	0.79 ± 0.01	830.20	0.98	20.5℃	39%
	01/03	2.08 ± 0.01	859.30	2.87	18.6℃	52%
	15/03	0.80 ± 0.01	894.30	0.90	21.5℃	31%
	29/03	2.05 ± 0.01	873.70	2.28	19.1℃	50%
	15/04	1.35 ± 0.01	909.30	1.00	18.5℃	40%
eel_100_1	08/02	1.30 ± 0.01	874.20	2.75	21.8℃	45%
	01/03	1.94 ± 0.01	898.67	0.94	18.6℃	52%
	15/03	0.82 ± 0.01	890.11	0.74	21.5℃	31%
	29/03	2.28 ± 0.01	867.78	1.81	19.1℃	50%
	15/04	2.03 ± 0.01	897.33	1.15	18.5℃	40%

Table 3.2.1: Potentiometer and sensor resistance values for 950sens and maximum applied pressure, in regard with the date of testing, temperature and humidity percentage for eel samples.

3.2.2.Pi-ETU samples

Sample	Date	Potentiometer Resistance Value (KΩ)	Max Resistance Value (sens)	Error (sens)	Temperature	Humidity
pi_1	21/03	9.90 ± 0.01	959.80	0.60	22.0℃	29%
	05/04	8.94 ± 0.01	967.70	0.46	22.0℃	42%
	20/04	11.11 ± 0.01	962.00	0.00	19.3℃	50%
	03/05	11.50 ± 0.01	954.20	0.40	21.0℃	45%
proto_ pi_1	21/03	2.11 ± 0.01	952.90	0.30	22.0℃	29%
	05/04	3.10 ± 0.01	955.10	0.30	22.0℃	42%
	20/04	3.85 ± 0.01	955.50	0.50	19.3℃	50%
	03/05	4.21 ± 0.01	958.20	0.60	21.0℃	45%
middle_ pi_1	21/03	1.58 ± 0.01	945.20	1.08	22.0℃	29%
	05/04	1.56 ± 0.01	951.10	0.54	22.0℃	42%
	20/04	1.55 ± 0.01	946.50	0.50	19.3℃	50%
	03/05	1.98 ± 0.01	947.10	0.30	21.0℃	45%
pi _20_1	22/02	2.82 ± 0.01	996.00	0.00	18.5℃	51%
	15/03	1.59 ± 0.01	964.50	0.50	21.5℃	31%
	29/03	1.84 ± 0.01	962.40	0.66	19.1℃	50%
	15/04	1.82 ± 0.01	953.80	0.40	18.5℃	40%
	03/05	3.34 ± 0.01	964.40	0.49	21.0℃	45%
pi _40_1	22/02	1.94 ± 0.01	989.20	0.60	18.5℃	51%
	15/03	0.96 ± 0.01	959.10	1.22	21.5℃	31%
	29/03	0.74 ± 0.01	927.40	0.66	19.1℃	50%
	15/04	1.06 ± 0.01	965.50	0.50	18.5℃	40%
	03/05	1.30 ± 0.01	954.80	0.49	21.0℃	45%
pi _60_1	22/02	1.05 ± 0.01	984.70	0.64	18.4℃	55%
	15/03	0.70 ± 0.01	964.50	0.67	21.5℃	31%
	29/03	1.11 ± 0.01	963.40	1.11	19.1℃	50%
	15/04	0.53 ± 0.01	965.80	0.40	18.5℃	40%
	03/05	0.77 ± 0.01	961.10	0.70	21.0℃	45%
pi _80_1	24/02	0.57 ± 0.01	967.00	0.00	18.5℃	55%
	15/03	0.56 ± 0.01	971.20	0.60	21.5℃	31%
	29/03	0.69 ± 0.01	952.30	0.46	19.1℃	50%
	15/04	0.75 ± 0.01	957.40	0.49	18.5℃	40%
	03/05	0.71 ± 0.01	940.10	0.70	21.0℃	45%
pi _100_1	24/02	11.20 ± 0.01	977.80	0.40	17.1℃	50%
	15/03	4.77 ± 0.01	949.00	0.00	21.5℃	31%
	29/03	7.80 ± 0.01	965.22	0.42	19.1℃	50%
	15/04	6.35 ± 0.01	969.00	0.00	18.5℃	40%
	03/05	6.90 ± 0.01	961.00	0.00	21.0℃	45%

Table 3.2.2: Potentiometer and sensor resistance values for 950sens and maximum applied pressure, in regard with the date of testing, temperature and humidity percentage for pi-etu samples.

3.2.3.Filaflex samples

Sample	Date	Potentiometer Resistance Value (KΩ)	Max Resistance Value (sens)	Error (sens)	Temperature	Humidity
fila_1	16/03	0.48 ± 0.01	954.80	0.40	21.5℃	31%
	01/04	1.34 ± 0.01	958.40	0.66	22.1℃	37%
	28/04	0.70 ± 0.01	957.90	0.70	22.0℃	29%
	09/05	1.28 ± 0.01	950.30	0.46	20.5℃	40%
proto_ fila _1	11/11	1.77 ± 0.01	949.40	0.49	21.5℃	31%
	16/03	1.10 ± 0.01	952.80	0.40	22.1℃	37%
	01/04	1.47 ± 0.01	951.50	0.50	22.0℃	29%
	28/04	1.21 ± 0.01	952.50	0.50	20.5℃	40%
middle_ fila _1	16/03	1.03 ± 0.01	949.20	0.60	21.5℃	31%
	01/04	1.77 ± 0.01	953.90	0.70	22.1℃	37%
	28/04	0.62 ± 0.01	956.80	0.40	22.0℃	29%
	09/05	2.40 ± 0.01	955.40	0.66	20.5℃	31%
fila _20_1	01/03	1.66 ± 0.01	979.80	0.40	18.6℃	52%
	16/03	1.55 ± 0.01	967.70	0.46	21.5℃	31%
	29/03	4.87 ± 0.01	947.00	0.63	19.1℃	50%
	20/04	1.52 ± 0.01	951.00	0.63	19.3℃	50%
	03/05	3.88 ± 0.01	948.10	0.70	21.0℃	45%
fila _40_1	02/03	0.84 ± 0.01	976.00	3.00	18.9℃	54%
	16/03	0.61 ± 0.01	958.10	0.54	21.5℃	31%
	29/03	1.21 ± 0.01	957.40	1.11	19.1℃	50%
	20/04	1.03 ± 0.01	931.50	0.92	19.3℃	50%
	03/05	1.30 ± 0.01	926.90	0.70	21.0℃	45%
fila _60_1	02/03	0.86 ± 0.01	988.10	0.30	17.4℃	60%
	16/03	0.54 ± 0.01	958.20	0.40	21.5℃	31%
	29/03	1.11 ± 0.01	970.10	0.54	19.1℃	50%
	20/04	1.52 ± 0.01	966.00	0.63	19.3℃	50%
	03/05	1.16 ± 0.01	942.20	0.98	21.0℃	45%
fila _80_1	08/03	0.72 ± 0.01	952.50	0.81	17.9℃	46%
	22/03	0.33 ± 0.01	960.60	0.49	22.0℃	33%
	11/04	1.29 ± 0.01	958.10	0.70	19.0℃	47%
	28/04	1.77 ± 0.01	955.20	0.60	22.0℃	29%
	09/05	0.77 ± 0.01	918.70	0.95	20.5℃	40%
fila _100_1	08/03	2.50 ± 0.01	980.90	0.30	20.4℃	49%
	22/03	1.59 ± 0.01	973.78	0.42	22.0℃	33%
	11/04	2.05 ± 0.01	976.33	0.47	19.0℃	47%
	28/04	2.17 ± 0.01	953.11	0.57	22.0℃	29%
	09/05	2.42 ± 0.01	939.70	0.95	20.5℃	40%

Table 3.2.3: Potentiometer and sensor resistance values for 950sensand maximum applied pressure, in regard with the date of testing, temperature and humidity percentage for filaflex samples.

4. Data Analysis

4.1. Transformation of units

It was previously mentioned and can be observed in the diagrams of *Section 3: Data Collection* [3] that the resistance values are not in S.I. units but in fixed resistance units that are characteristic to the data collection set up. Furthermore, the x-axis of each diagram is the weight and not the collective pressure applied on the sensor.

4.1.1. Weight to pressure.

Even though the pressure as proportional to the weight applied since the sensor dimensions are kept unchanged, for consistence reasons the x-axis was changed to pressure. For the calculation of applied the gravitational acceleration was set at the defines by the 3rd CGPM (1901) standard, $9.81 \pm 0.1 \frac{m}{s^2}$. As the weight error, the minimal subdivision of the values was chosen, as shown on *Table 4.1.1*. The radius of the sensor, transformed to S.I. units along with the corresponding error is:

$$Radius\ (m) = 7.25 \pm 0.01(mm) * 10^{-3} = 0.007250 \pm 0.000010\ (m) \quad (4.1.1)$$

Therefore, the surface *A* is*:*

$$Surface\ (m^2) = \pi * ((7.25 \pm 0.01)(mm) * 10^{-3})^2 = 0.0001651 \pm 0.0000046\ (m^2)$$

The force applied on top of the sensor results from:

$$Force\ (N) = (9.81 \pm 0.10)\left(\frac{m}{s^2}\right) * (Weight \pm 0.10)(Kg) \quad (4.1.3)$$

The applied pressure in MPa is calculated according to the following formula:

$$Pressure\ (MPa) = \frac{Force \pm \delta Force(N)}{Surface \pm 0.0000046(m^2)} * 10^{-6} \quad (4.1.4)$$

The corresponding errors of every measurement were calculated with the following formula:

$$\delta f = \sqrt{\left(\frac{\partial f}{\partial a}\right)^2 + \left(\frac{\partial f}{\partial b}\right)^2 + \cdots} \quad (4.1.5)$$

Therefore, the resulting table regarding the transformation of weight values to pressure in MPa, is the following:

Weight (Kg)	Force (N)	Error (N)	Pressure (MPa)	Error (MPa)
0.7	6.87	0.69	0.042	0.004
1.7	16.68	1.67	0.101	0.010
2.7	26.49	2.65	0.160	0.016
3.7	36.30	3.63	0.220	0.022
4.7	46.11	4.61	0.279	0.028
6.7	65.73	6.57	0.398	0.040
8.7	85.35	8.54	0.517	0.052
10.7	104.97	10.50	0.636	0.064
12.7	124.59	12.46	0.754	0.075
14.7	144.21	14.42	0.873	0.087

Table 4.1.1: Pressure values and corresponding errors in MPa in regard to weight values.

4.1.2.Arduino resistance values to Ohm.

In order to have insight on how the sample resistance changes, the fixed values that were collected have to be transformed to S.I. resistance values, with the voltage divider formula shown below.

$$Resistance\ (K\Omega) = R_{pot}\ (K\Omega)\left(\frac{V_{in}\ (V)}{V_{out}(V)} - 1\right) \tag{4.1.6}$$

In *Formula 4.1.6,* Vin is the inserted voltage in the circuit. V_{in} corresponds to $1023sens$ which is the max value of the Arduino circuit without connecting the potentiometer and is equal to $5.00 \pm 0.01V$. V_{out} is the voltage that passes through the senor and it is derived from the sens value of the resistance in each case as shown in *Formula 4.1.7*

$$V_{out} = \frac{Resistance \pm stdev(sens) * 5.00 \pm 0.01\ (V)}{1023(sens)} \tag{4.1.7}$$

4.1.3.Data analysis.

As is previously mentioned, the average resistance values for maximum and minimum pressure applied were derived by calculating the average of 10 consecutive maximum and minimum peaks of the response diagram for each sample as shown in *Figure 3.2.1* and *Figure 3.2.2.*

With close observation of the resulting resistance values that correspond to zero pressure applied on the samples, it is noted that there are significant differences between them, despite the fact that the samples remained in a fixed position. Since when any amount of pressure is applied on the sensors, the material is deformed and with the pressure lifted, they return to their original state, the differences in the resistance values that correspond to that point, appear to occur due to an abnormal return of the material to its original shape and due to the fact that the oscillation frequency has errors and is not fixed to accommodate each sample respectively.

As a result, the resistance values obtained do not represent the true initial resistance of each sample, which should be constant. Therefore, in order to test the resistivity of each sample, the resistance values that correspond to the minimum peaks of the response diagram were not taken into consideration in the final Resistance – Pressure diagrams, since if the initial constant resistance, measured when zero amount of pressure is applied is subtracted from the existing resistance values that correspond to the maximum peaks, we will result in a curve with the same slope but with a different starting point, therefore not changing which sample is optional.

In order to compare the individual Resistance-Pressure diagrams of each sample, the resistance values have to be normalized. The normalization was concluded between 0 and 1, according to *Formula 4.1.8.*

$$Normalized\ R = \frac{r - Min}{max - \min} \tag{4.1.8}$$

4.2. Data analysis for original measurements.

Taking into consideration *Formula 4.1.6, Formula 4.1.7* and *Table 4.1.1* along with the measured resistance values for each sample as shown in Appendix 1, we result in the Resistance – Pressure diagrams that contain the average resistance values in regard to pressure applied for each sample. Using *Origin,* for each diagram the fitting curve was designed.

4.2.1.Ninjatek eel samples

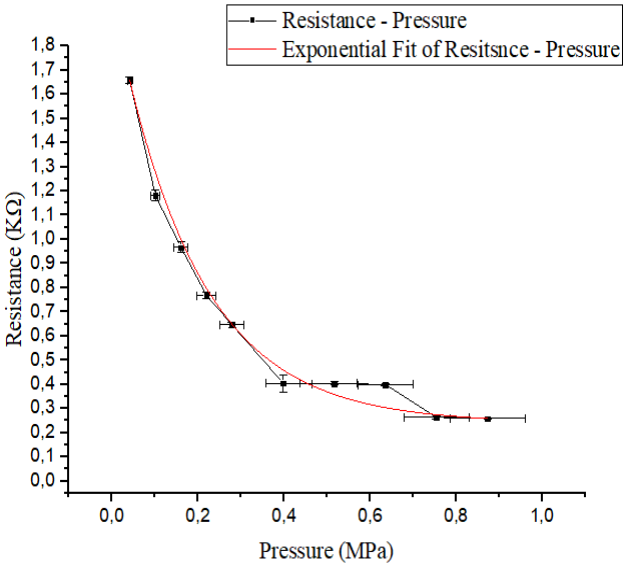

Figure 4.2.1: Resistance-Pressure curve and exponential fit for average resistance values of single filament eel sensors

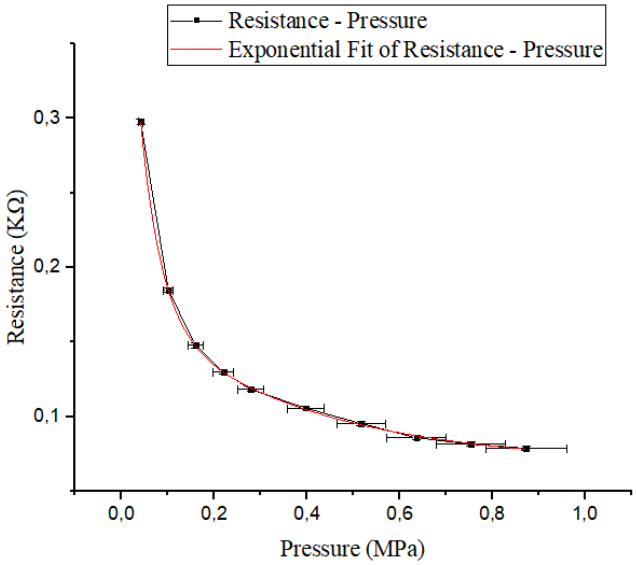

Figure 4.2.2: Resistance-Pressure curve and exponential fit for average resistance values of eel sensors with two protopasta layers.

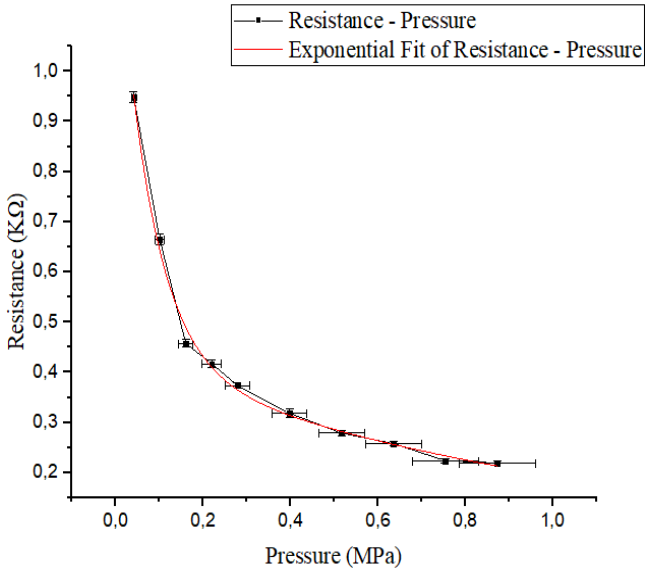

Figure 4.2.3: Resistance-Pressure curve and exponential fit for average resistance values of eel sensors with three protopasta layers.

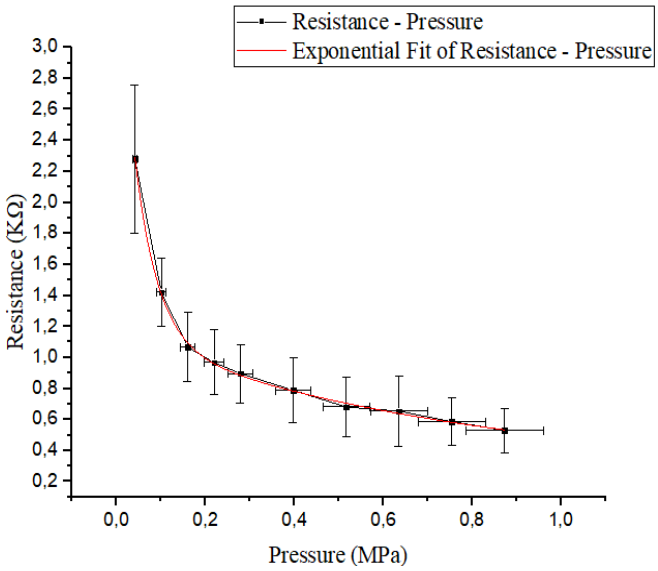

Figure 4.2.4: Resistance-Pressure curve and exponential fit for average resistance values of for eel sensors with 20% infill.

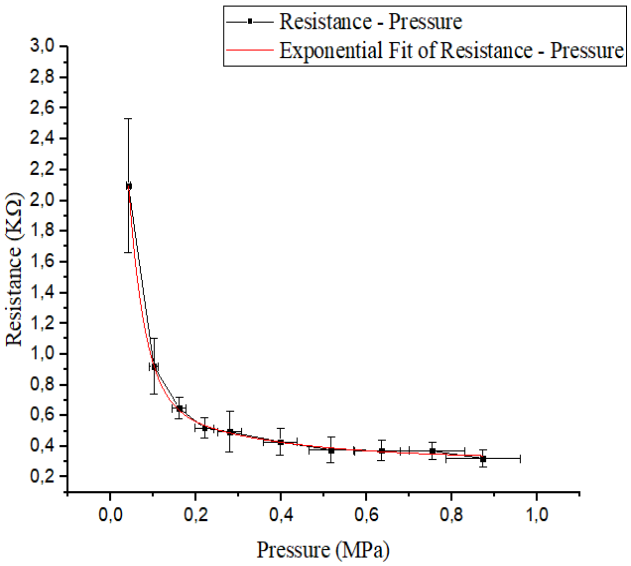

Figure 4.2.5: Resistance-Pressure curve and exponential fit for average resistance values of eel sensors with 40% infill.

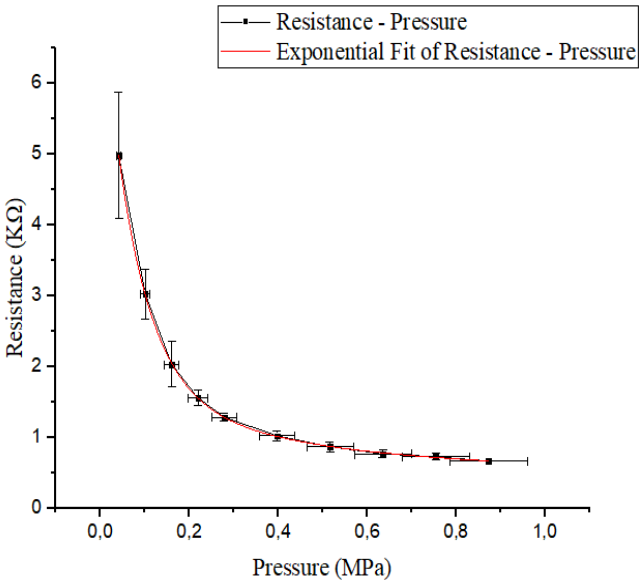

Figure 4.2.6: Resistance-Pressure curve and exponential fit for average resistance values of eel sensors with 60% infill.

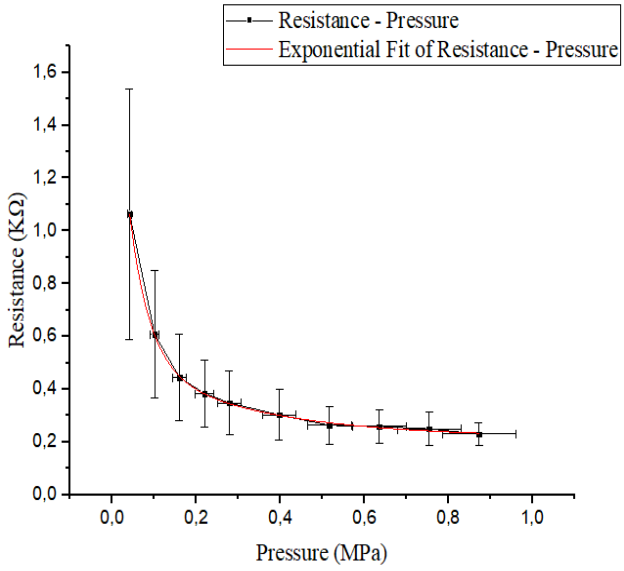

Figure 4.2.7: Resistance-Pressure curve and exponential fit for average resistance values of eel sensors with 80% infill.

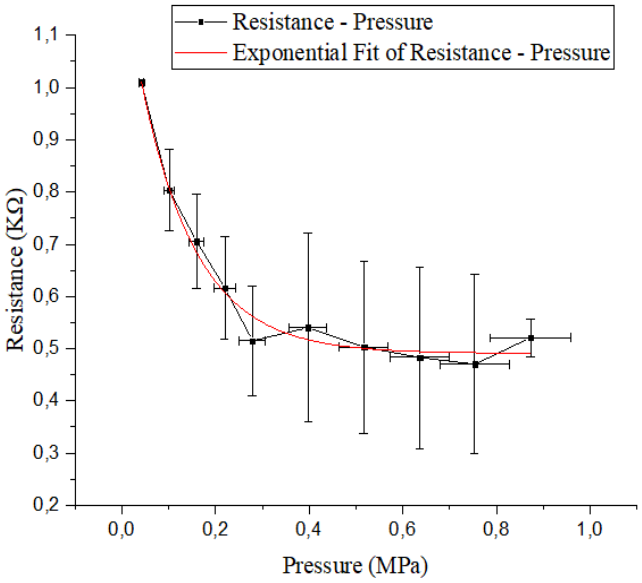

Figure 4.2.8: Resistance-Pressure curve and exponential fit for average resistance values of eel sensors with 100% infill.

4.2.2.Pi – ETU samples.

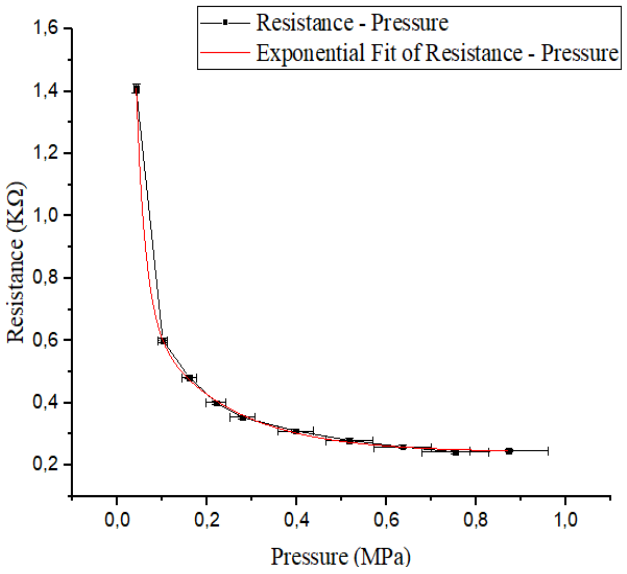

Figure 4.2.9: Resistance-Pressure curve and exponential fit for average resistance values of single filament pi-etu sensors

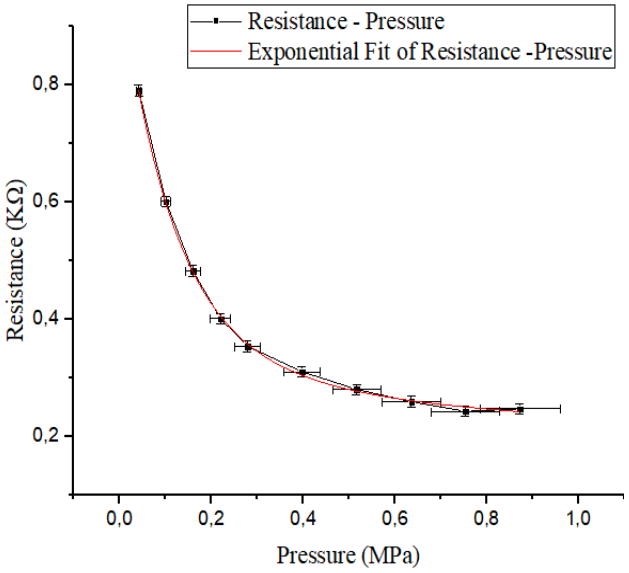

Figure 4.2.10: Resistance-Pressure curve and exponential fit for average resistance values of pi-etu sensors with two protopasta layers.

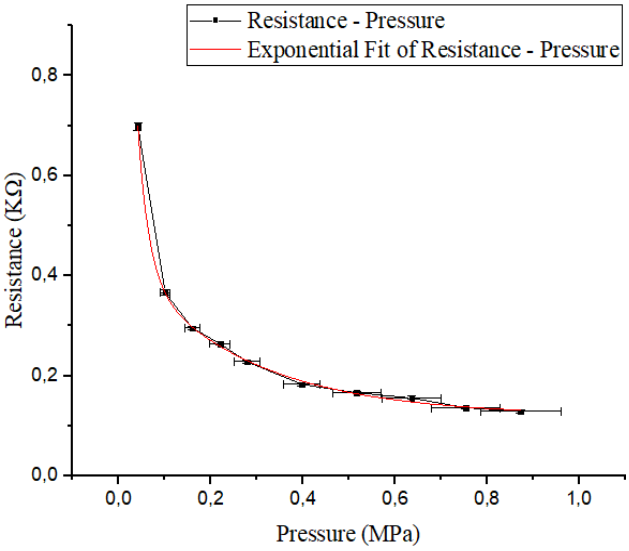

Figure 4.2.11: Resistance-Pressure curve and exponential fit for average resistance values of pi-etu sensors with three protopasta layers.

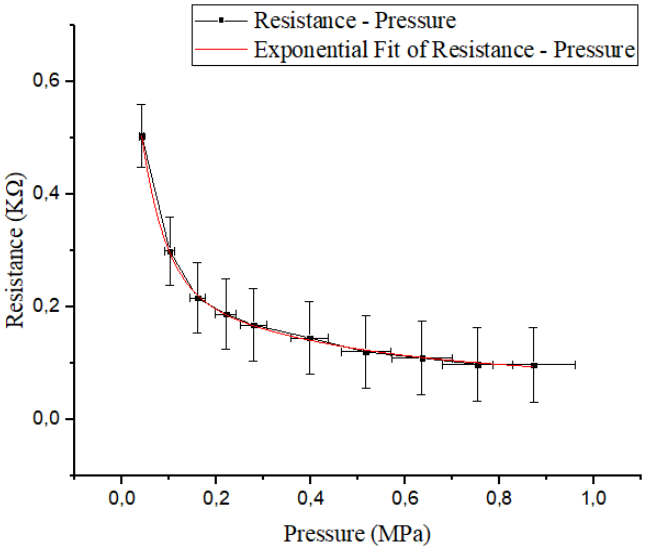

Figure 4.2.12: Resistance-Pressure curve and exponential fit for average resistance values of pi-etu sensors with 20% infill.

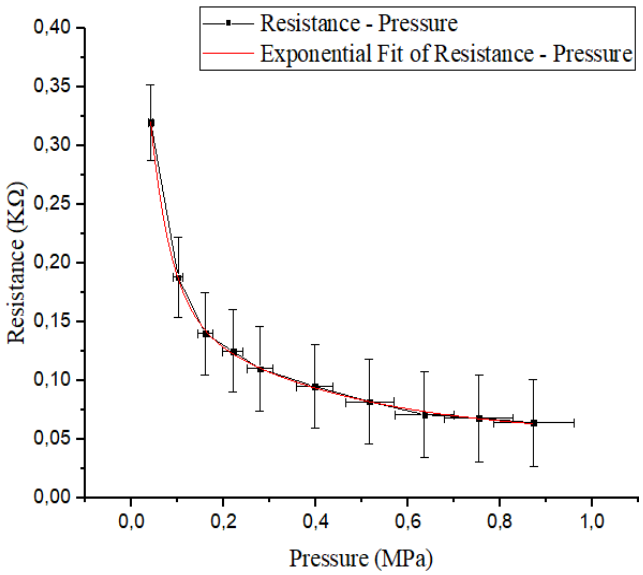

Figure 4.2.13: Resistance-Pressure curve and exponential fit for average resistance values of pi-etu sensors with 40% infill.

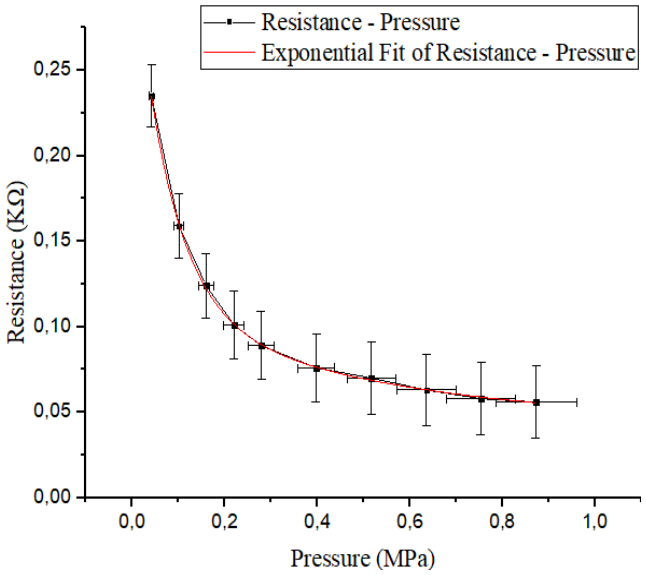

Figure 4.2.14: Resistance-Pressure curve and exponential fit for average resistance values of pi-etu sensors with 40% infill

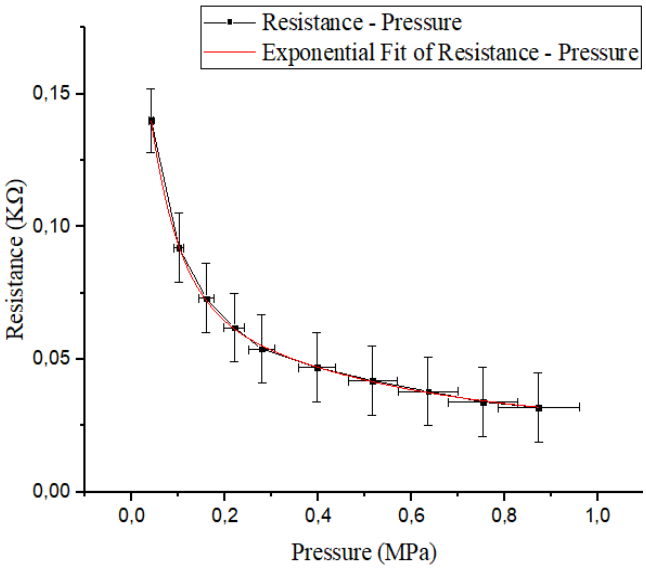

Figure 4.2.15: Resistance-Pressure curve and exponential fit for average resistance values of pi-etu sensors with 40% infill.

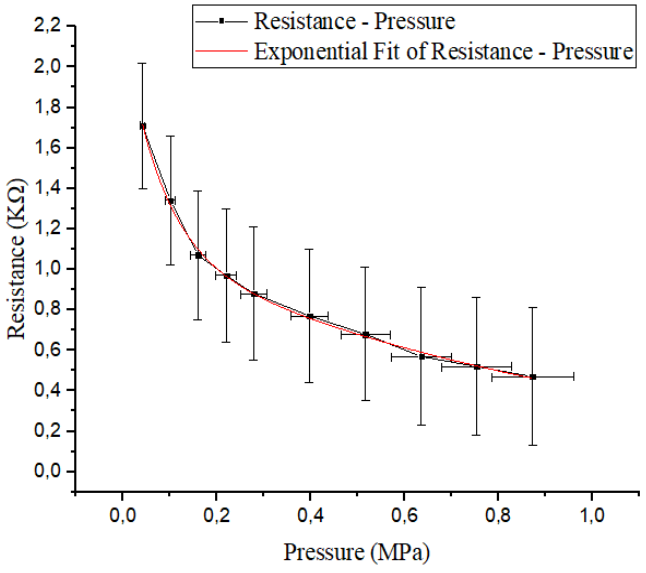

Figure 4.2.16: Resistance-Pressure curve and exponential fit for average resistance values of pi-etu sensors with 100% infill.

4.2.3.Filaflex samples

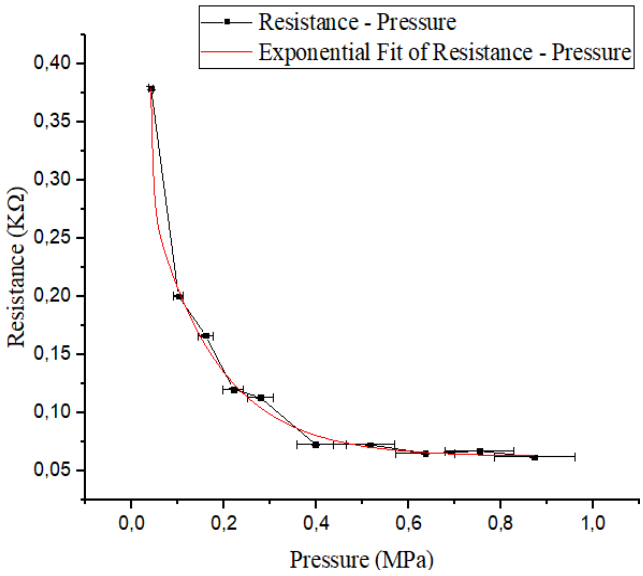

Figure 4.2.17: Resistance-Pressure curve and exponential fit for average resistance values of single filament filaflex sensors.

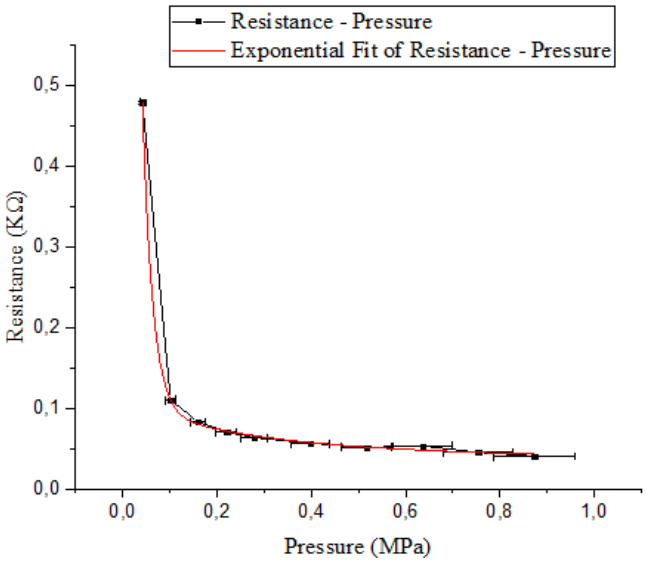

Figure 4.2.18: Resistance-Pressure curve and exponential fit for average resistance values of filaflex sensors with two protopasta layer.

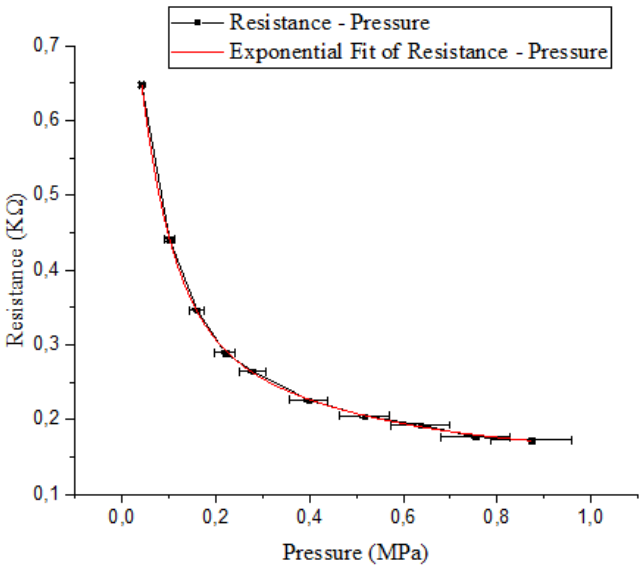

Figure 4.2.19: Resistance-Pressure curve and exponential fit for average resistance values of filaflex sensors with three protopasta layers

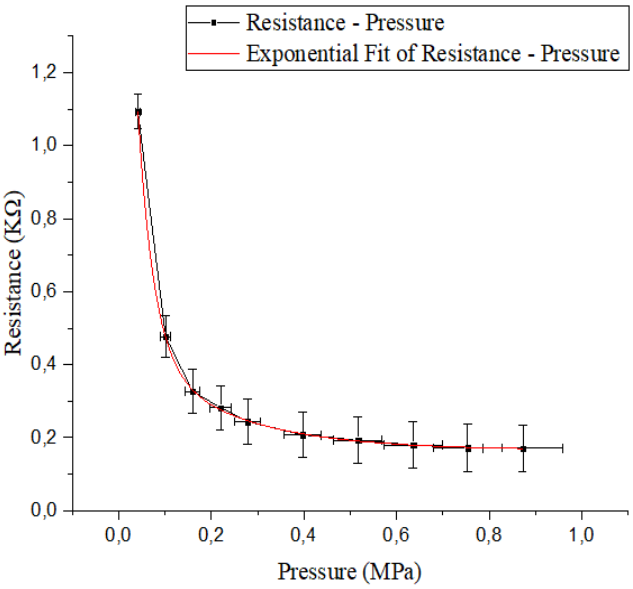

Figure 4.2.20: Resistance-Pressure curve and exponential fit for average resistance values of filaflex sensors with 20% infill

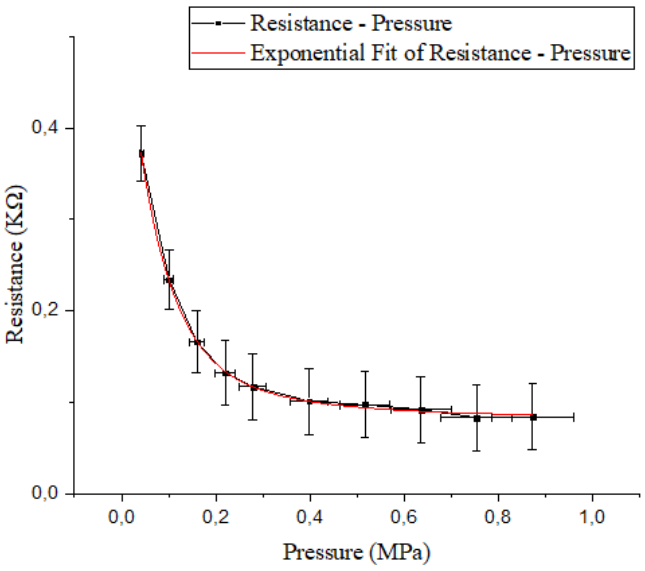

Figure 4.2.21: Resistance-Pressure curve and exponential fit for average resistance values of filaflex sensors with 40% infill.

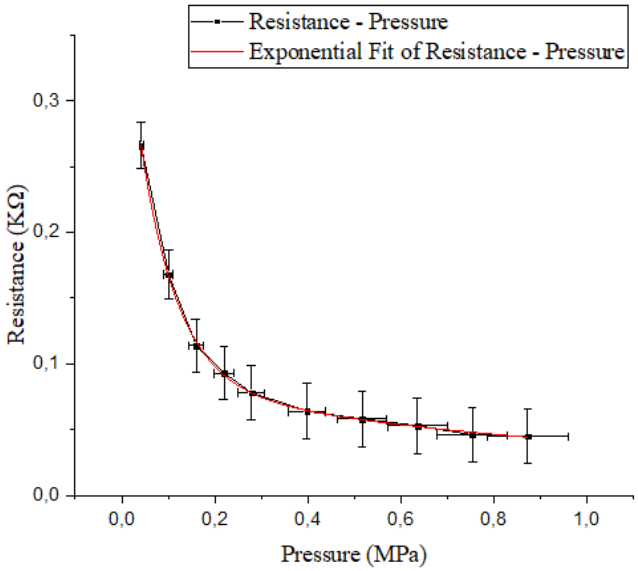

Figure 4.2.22: Resistance-Pressure curve and exponential fit for average resistance values of sensors with 60% infill

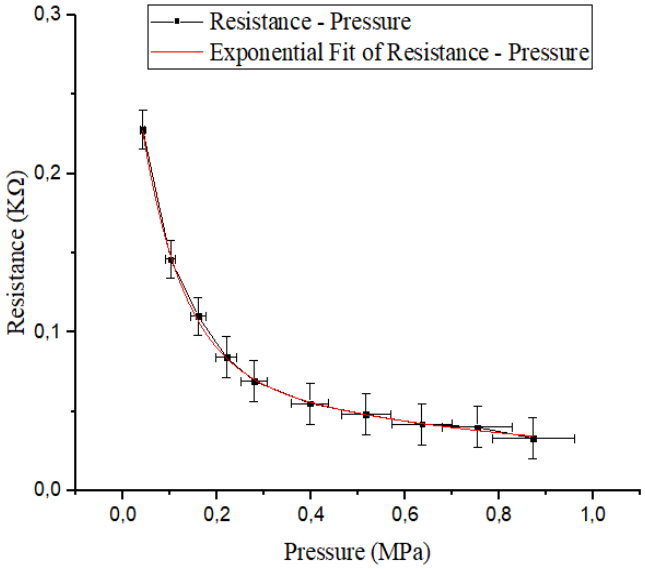

Figure 4.2.23: Resistance-Pressure curve and exponential fit for average resistance values of filaflex sensors with 80% infill.

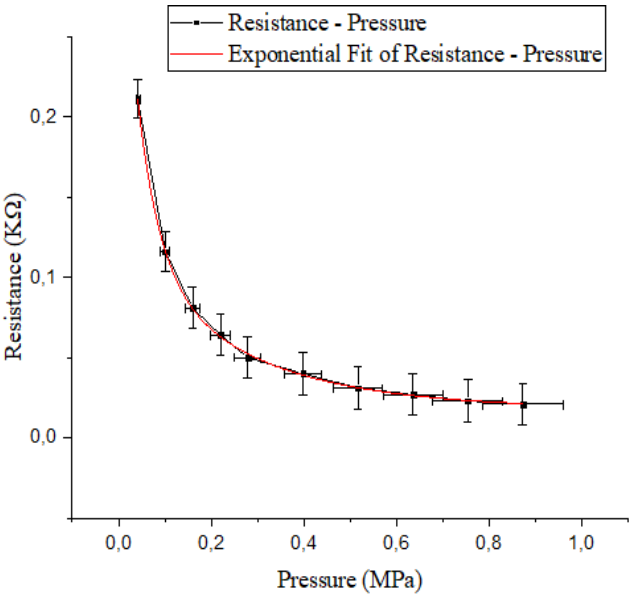

Figure 4.2.24: Resistance-Pressure curve and exponential fit for average resistance values of filaflex sensors with 100% infill

4.2.4. Comparison and results

As shown above, the data collected from the gait simulation were transformed into resistance values, and for each sample, the corresponding Resistance – Pressure diagram was created. After fitting, which was done using the tools provided by *Origin* it was concluded that the most suitable formula to describe how the sample resistance changes as pressure is applied, is the two-phase exponential decay formula, with added offset (y_0) for optimized fitting. The reason is that as it can be observed in the majority of the diagrams, after the pressure applied surpasses the point of $0.220 \pm 0.022\ MPa$ the diagram appears to be less steep and the resistance values that correspond to the following pressure values seem to be quite similar. The two exceptions are the single filament eel sample (eel_i) and the 100% infill eel sample (eel_100_i) where the one phase-exponential decay formula seems to better describe the changes in the samples' resistance as pressure is applied (*Figure 4.5.2).*

The purpose of the fitting process therefore, using the t, t_1 and t_2 parameters that are automatically calculated during the fitting process, is to indicate the decay rate factors, $k_i = -1/_{t_i}$ that signify how steep the curve will be and therefore how fast the resistance of the sample in question changes as pressure is applied. It is noted that the main contributor to the steepness of the curve is the fast decay rate when the formula used for fitting is the two-phase exponential decay one. Since the decay rate is negative, the steepest curve, and therefore the sensor with the highest sensitivity should be the one with the highest absolute decay rate value. Furthermore, as the fitting was completed with the existing tools from the *Origin* software, in the exponential decay formula provided, the independent variable was set in time units, which was changed to accommodate the current study, in which the independent variable is Pressure (MPa), as shown in *Formula 4.5.1*. The use of a set fitting formula, facilitated the calculation of the A, B and C in the one-phase exponential decay case, constants which indicate the resistance value when pressure is zero and therefore the initial point of the curve following the fast decay rate, and the initial point of the curve following the slow decay rate respectively.

$$Resistance(P) = A \cdot (K\Omega)e^{-\left(P/t_1\right)} + B \cdot (K\Omega)e^{-\left(P/t_1\right)} + y_0 \quad (4.5.1)$$

$$Resistance(P) = C \cdot (K\Omega)e^{-\left(P/t\right)} + y_0 \quad (4.5.2)$$

In order to reach a conclusion about which sample is optimal, we should take into consideration that the slow decay rate is that that refers to higher amounts of pressure while the fast decay rate, in most cases, refers to pressure amounts close to zero. An interesting observation is that the measurements that correspond to higher pressures seem to have smaller errors, an indicator that the gait simulator set up could affect the results negatively in lower pressures and therefore the resulting fast decay rates may differ from reality. In order for the results to be more accurate, apart from comparing the collective decay rates for the samples, three collective Resistance – Pressure diagrams were created, each containing the average, normalized resistance values of all the samples printed with a specific filament.

The collective decay rates for each one of the samples are shown in *Table 4.2.1* As mentioned, the decay rate indicates the steepness of the Resistance-Pressure curve, and therefore the sensitivity of the tested sensor. Since the decay rate values are negative, the smaller the decay rate is, the steepest the corresponding curve will be. Therefore, the sample with the smallest decay rate, will be the one with the highest sensitivity to pressure changes. In *Figure 4.2.25,* the collective Resistance-Pressure diagram for all the sensors is shown. Since the sole purpose of *Figure 4.2.25* is to visualize the results derived from *Table 4.2.1,* the error bars are not included in order to have a clearer view of the steepness of the depicted curves. The same collective diagram is depicted and further discussed in *Figure 5.2.3.* in *Section 5: Conclusion/Discussion* [(5)] where error bars have been added.

Eel samples	**Fast decay rate k_1 (MPa^{-1})**	**Slow decay rate (MPa^{-1})**
Single filament	-5.84 ± 0.52	–
Two protopasta layers	-22.66 ± 1.41	-2.72 ± 0.33
Three protopasta layers	-12.98 ± 3.54	-1.78 ± 1.69
20% infill	-19.96 ± 2.24	-1.41 ± 0.69
40% infill	-26.31 ± 2.56	-3.57 ± 1.41
60% infill	-13.07 ± 0.48	-3.57 ± 1.40
80% infill	-20.66 ± 4.11	-3.23 ± 1.02
100% infill	-8.40 ± 0.71	–
Pi-ETU samples	**Fast decay rate k_1 (MPa^{-1})**	**Slow decay rate (MPa^{-1})**
Single filament	-48.781 ± 0.093	-5.556 ± 0.065
Two protopasta layers	-8.85 ± 2.04	-1.97 ± 3.61
Three protopasta layers	-41.67 ± 10.42	-3.89 ± 0.55
20% infill	-20.08 ± 2.17	-2.56 ± 0.79
40% infill	-22.79 ± 0.22	-2.60 ± 0.52
60% infill	-12.74 ± 1.15	-1.88 ± 0.92
80% infill	-16.84 ± 1.67	-2.27 ± 0.57
100% infill	-12.50 ± 3.12	-0.91 ± 1.06
Filaflex samples	**Fast decay rate k_1 (MPa^{-1})**	**Slow decay rate (MPa^{-1})**
Single filament	-204.08 ± 400.00	-6.67 ± 1.47
Two protopasta layers	-49.30 ± 5.14	-3.23 ± 1.25
Three protopasta layers	-14.81 ± 1.29	-2.65 ± 0.60
20% infill	-29.15 ± 0.15	-4.95 ± 0.57
40% infill	-26.17 ± 2.54	-3.57 ± 1.40
60% infill	-13.07 ± 0.48	-2.41 ± 0.57
80% infill	-11.91 ± 1.87	-1.84 ± 1.93
100% infill	-21.18 ± 2.20	-3.95 ± 0.61

Table 4.2.1: Decay rates for each one of the samples. The smallest decay rate indicates the sensor with the highest sensitivity.

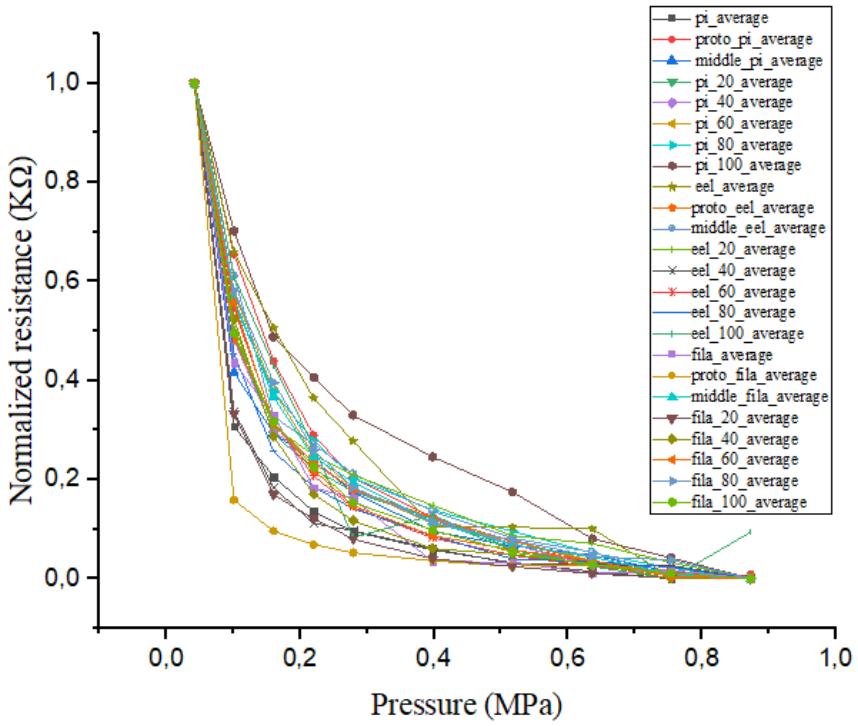

Figure 4.2.25: The indicative collective Resistance-Pressure diagram for all the samples. The error bars are not shown in order to have a clearer view of the curves depicted.

While according to the data showcased in *Table 4.2.1* it is proposed that the steepest curve should belong to the single filament filaflex samples, *Figure 4.2.25* contradicts this claim, since the steepest curve belongs to the filaflex samples with two added protopasta layers.

4.3. Aging analysis.

In the aging tests, since data for each sample were collected only for $14.7 \pm 0.01\ Kg$, according to *Table 4.1.1*, the pressure applied on the sensors equals to $0.873 \pm 0.087\ MPa$. Taking into consideration the dates and measured resistance values shown in *Section 3: Data Collection* [3] after transforming the resistance values in KΩ according to *Formula 4.1.6.*, the Resistance – Dates diagrams for each sample are designed created.

4.3.1.Ninjatek eel samples

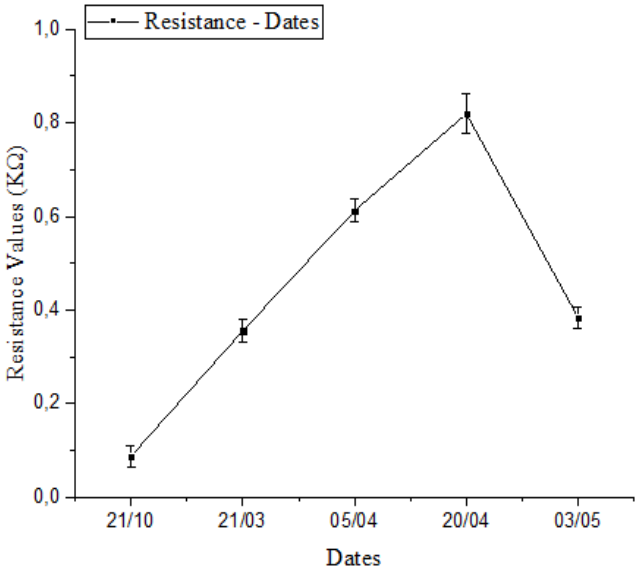

Figure 4.3.1: Resistance – Dates diagram for the single filament eel sample.

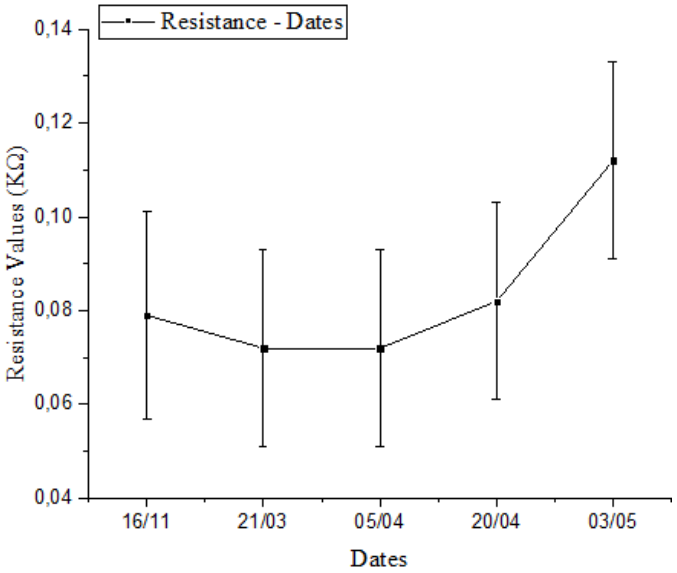

Figure 4.3.2: Resistance – Dates diagram for the eel sample with two protopasta layers.

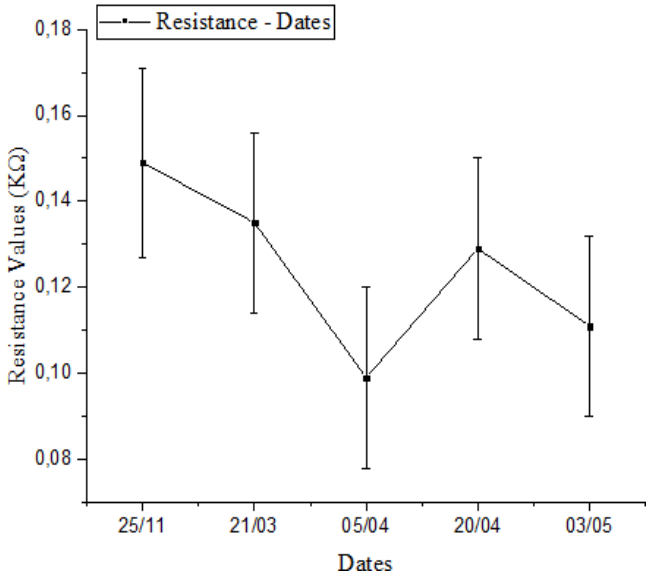

Figure 4.3.3: Resistance – Dates diagram for the eel sample with three protopasta layers.

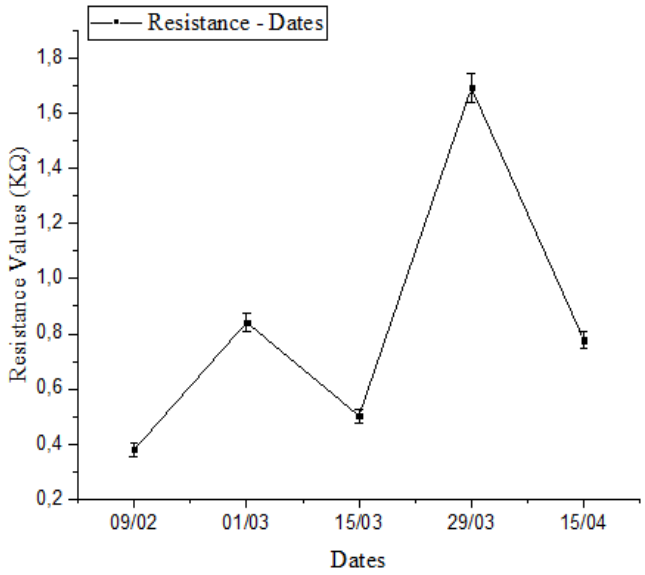

Figure 4.3.4: Resistance – Dates diagram for the eel sample with 20% infill.

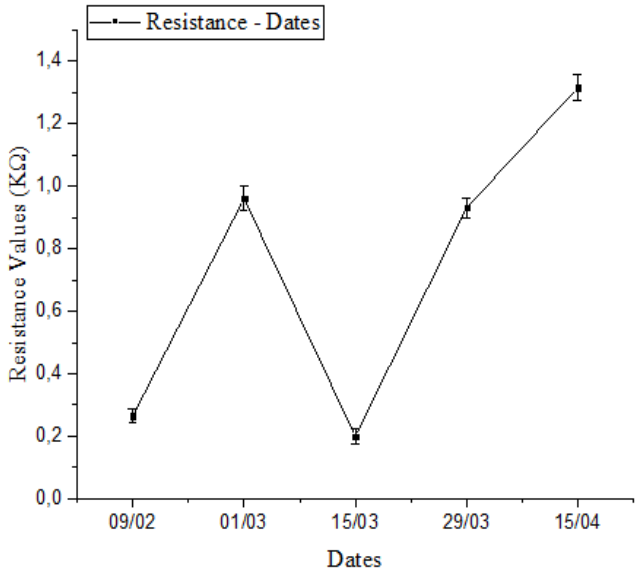

Figure 4.3.5: Resistance – Dates diagram for the eel sample with 40% infill.

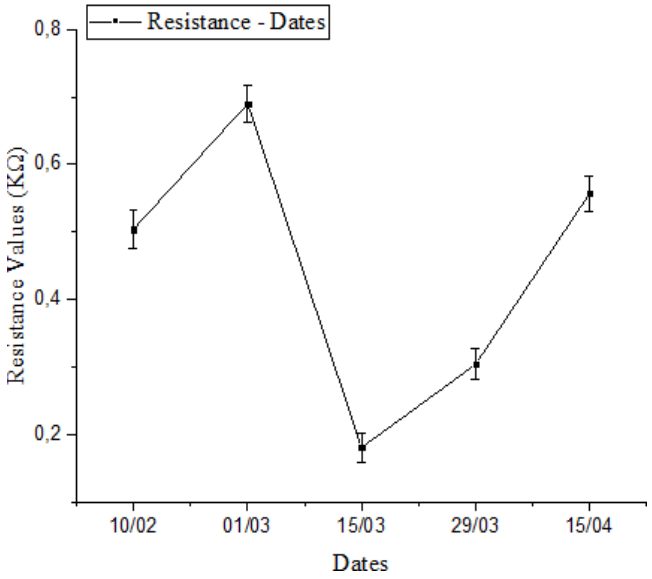

Figure 4.3.6: Resistance – Dates diagram for the eel sample with 60% infill.

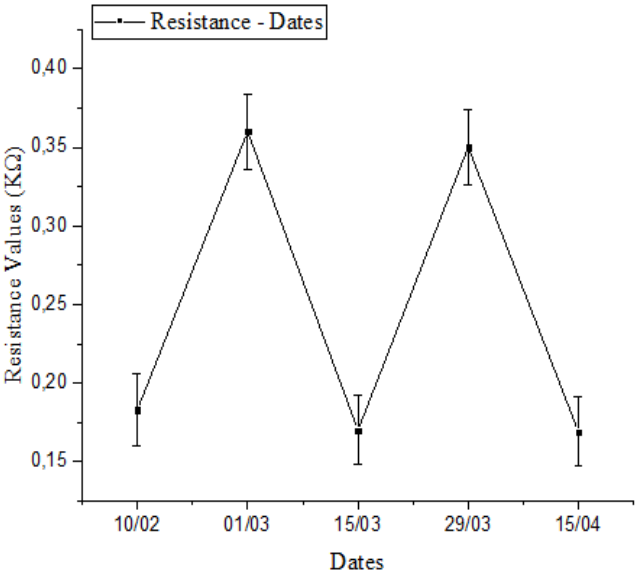

Figure 4.3.7: Resistance – Dates diagram for the eel sample with 80% infill.

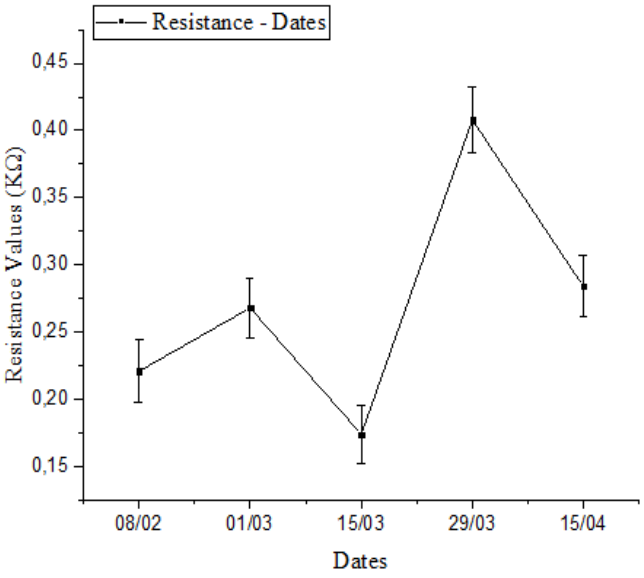

Figure 4.3.8: Resistance – Dates diagram for the eel sample with 100% infill.

4.3.2.Pi-ETU samples

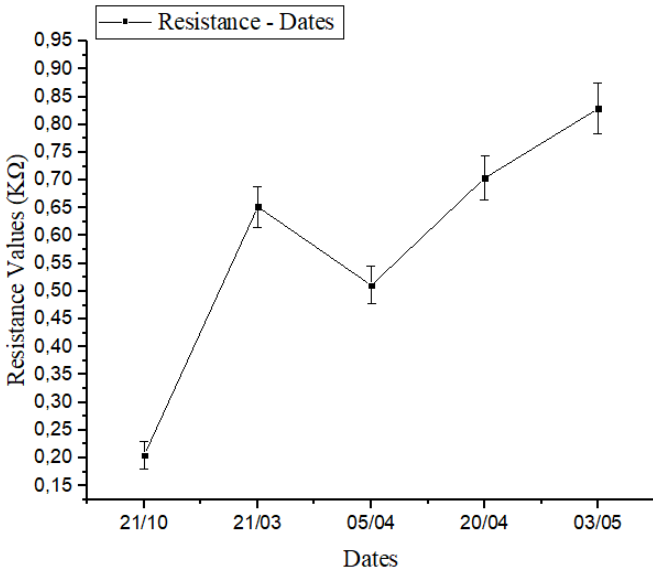

Figure 4.3.9: Resistance – Dates diagram for the single filament pi-etu sample.

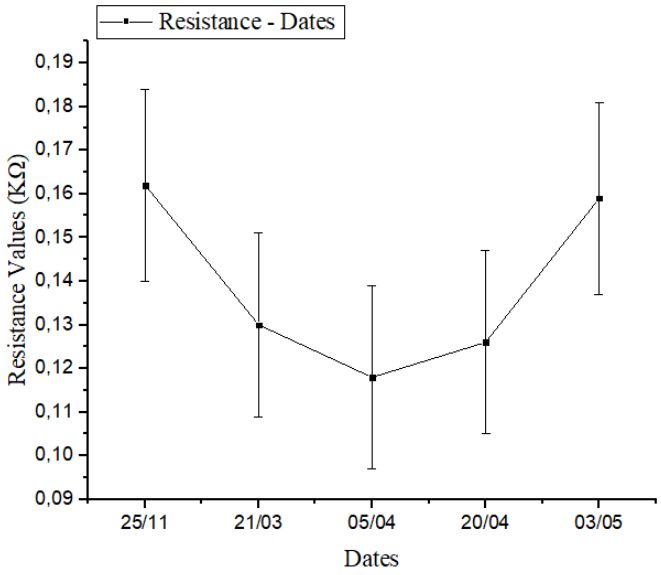

Figure 4.3.10: Resistance – Dates diagram for the pi-etu sample with two protopasta layers.

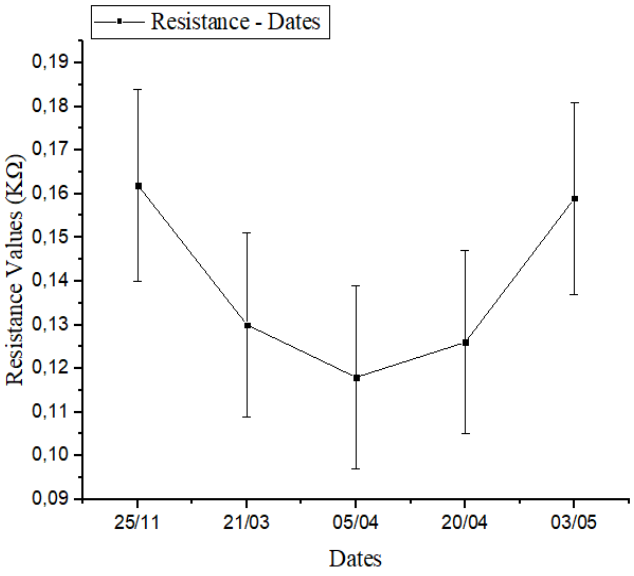

Figure 4.3.11: Resistance – Dates diagram for the pi-etu sample with three protopasta layers.

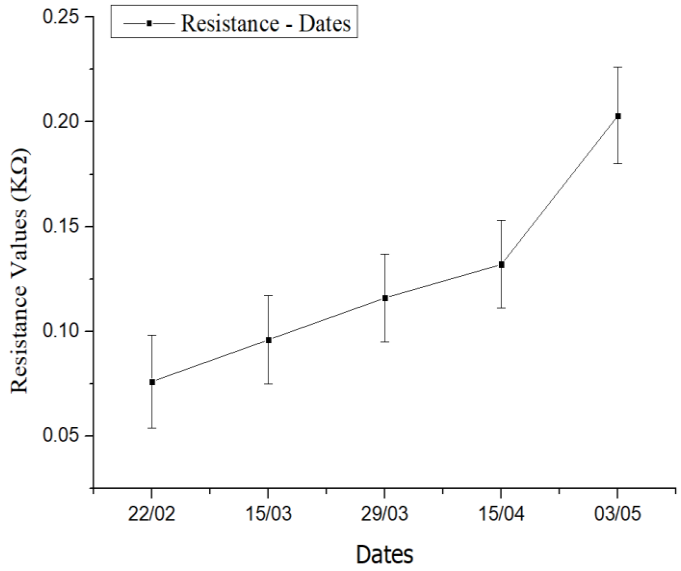

Figure 4.3.12: Resistance – Dates diagram for the pi-etu sample with 20% infill.

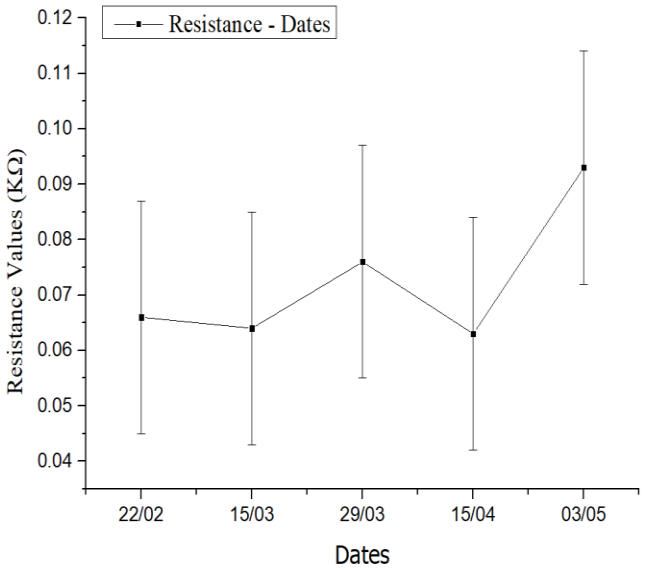

Figure 4.3.13: Resistance – Dates diagram for the pi-etu sample with 40% infill.

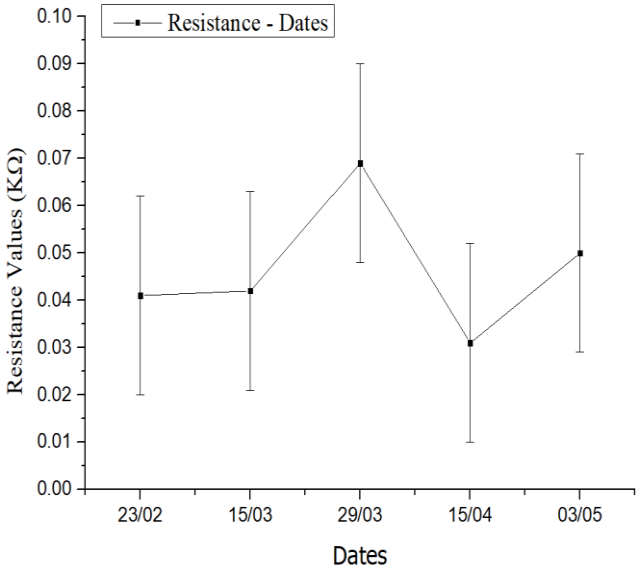

Figure 4.3.14: Resistance – Dates diagram for the pi-etu sample with 60% infill.

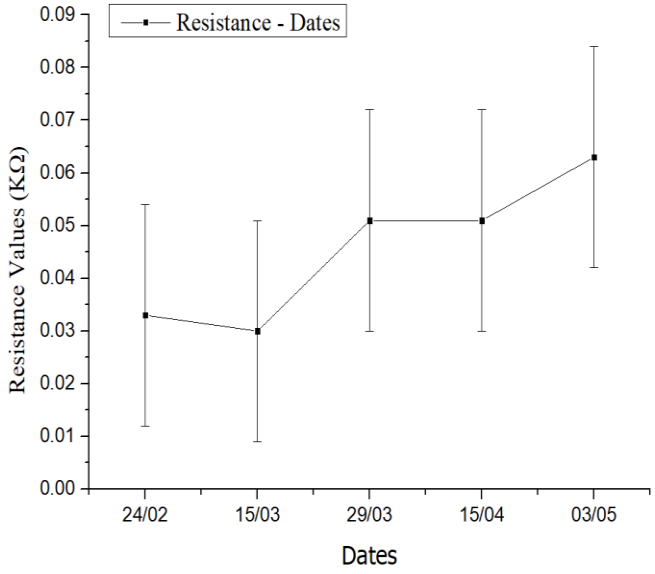

Figure 4.3.15: Resistance – Dates diagram for the pi-etu sample with 80% infill.

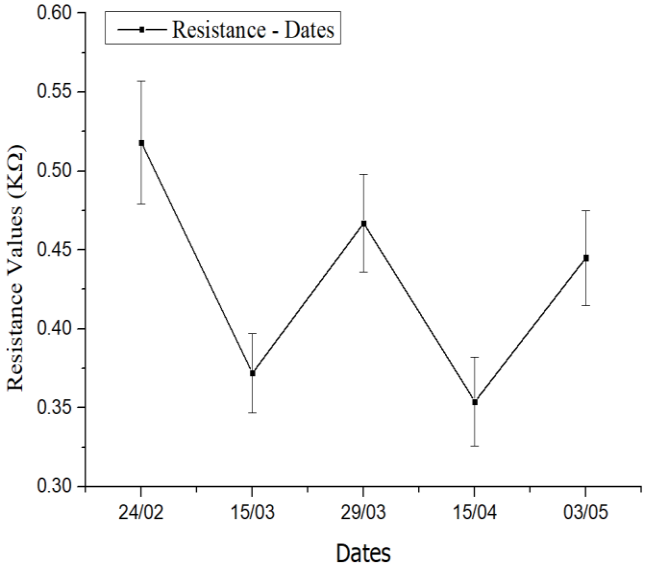

Figure 4.3.16: Resistance – Dates diagram for the pi-etu sample with 100% infill.

4.3.3.Filaflex samples

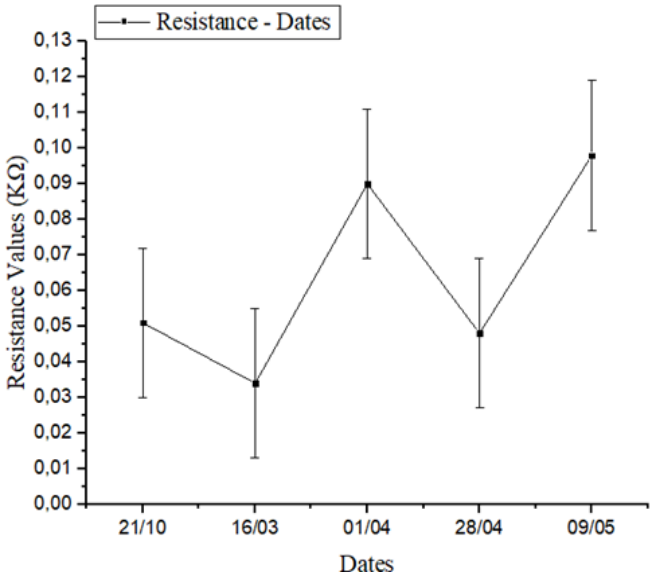

Figure 5.3.17: Resistance – Dates diagram for the single filament filaflex sample.

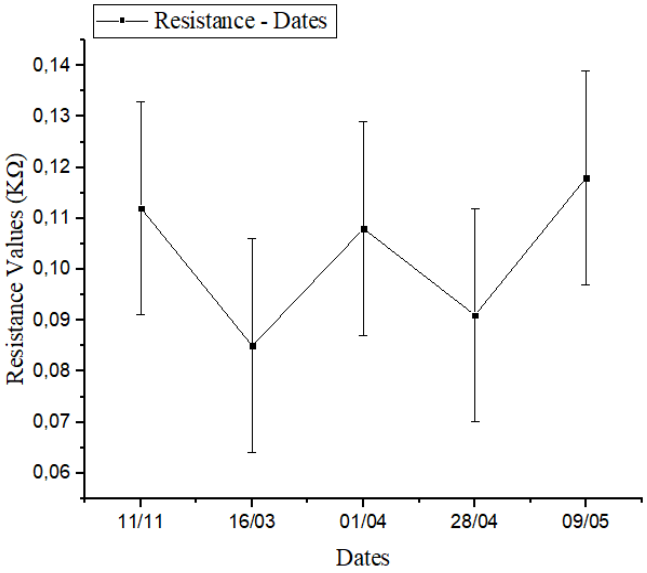

Figure 4.3.18: Resistance – Dates diagram for the filaflex sample with two protopasta layers.

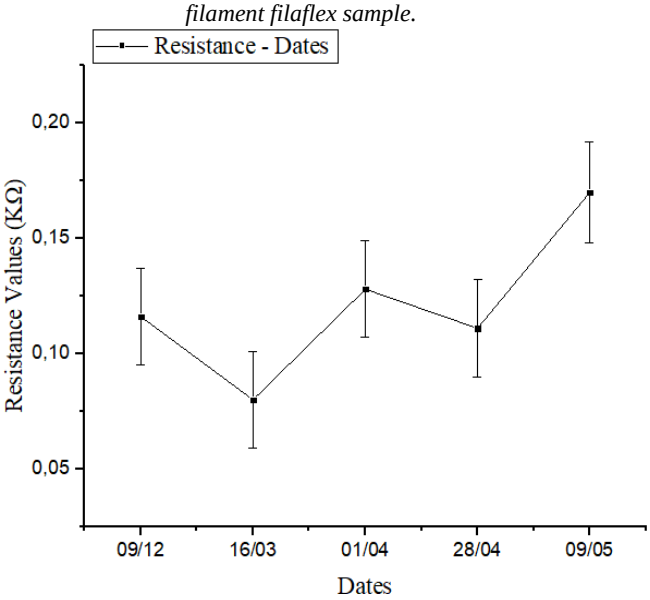

Figure 4.3.19: Resistance – Dates diagram for the filaflex sample with three protopasta layers.

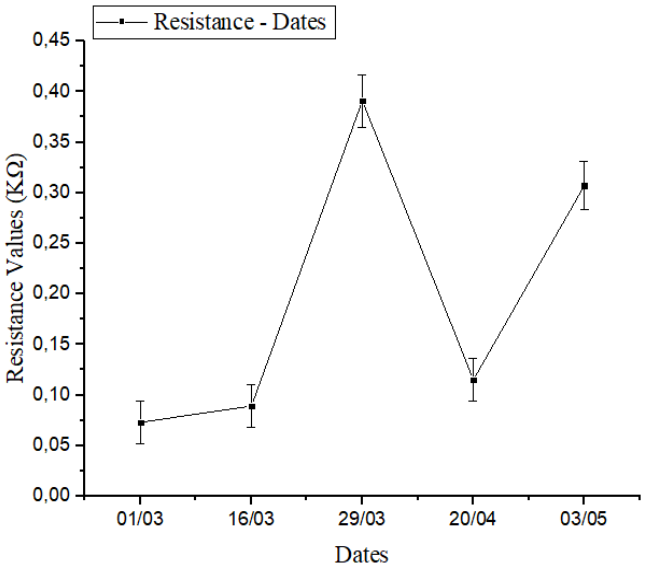

Figure 4.3.20: Resistance – Dates diagram for the filaflex sample with 20% infill.

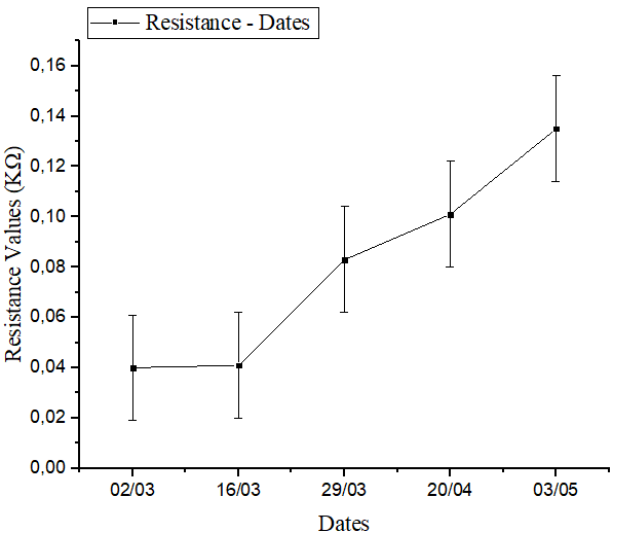

Figure 4.3.21: Resistance – Dates diagram for the filaflex sample with 40% infill.

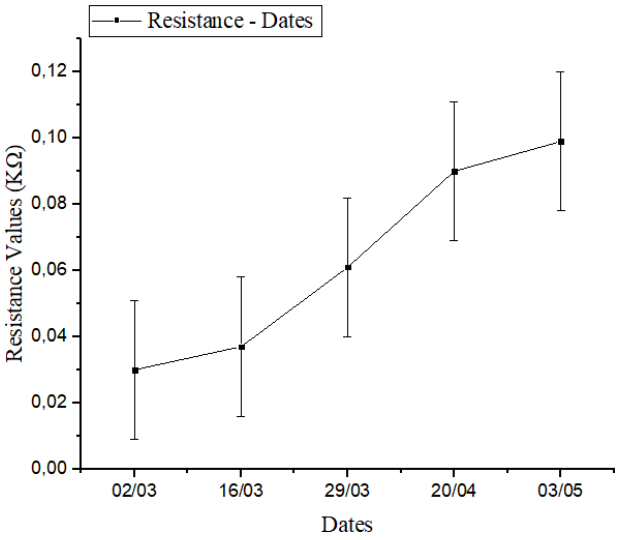

Figure 4.3.22: Resistance – Dates diagram for the filaflex sample with 60% infill.

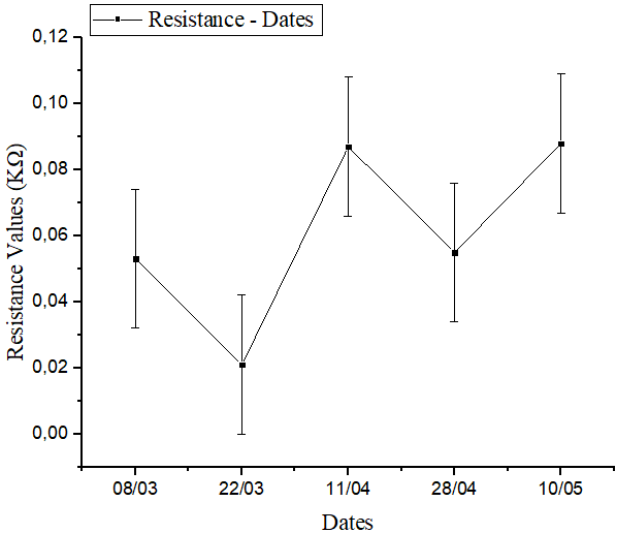

Figure 4.3.23: Resistance – Dates diagram for the filaflex sample with 80% infill.

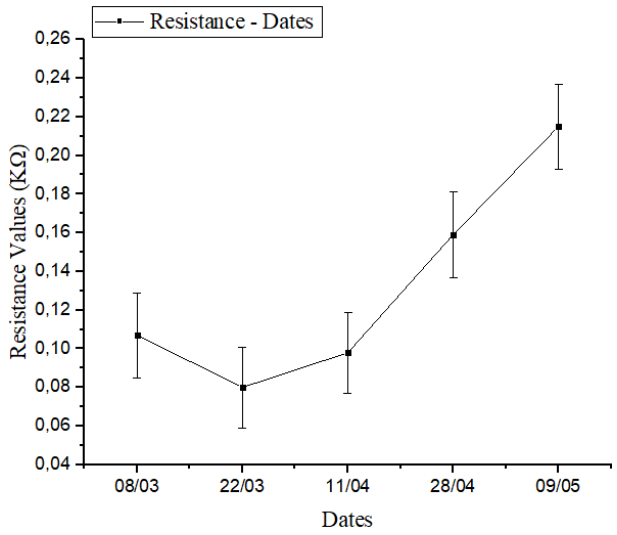

Figure 4.3.24: Resistance – Dates diagram for the filaflex sample with 100% infill.

4.3.4.Results

Taking into consideration *Table 3.2.2* after comparing the Resistance-Dates diagrams, it appears that humidity and temperature affect the changes in sensor sensitivity, based on the measured resistance values for maximum pressure applied. How humidity and temperature affect each sensor and how major or minor is each factor's contribution to the changes in sensor sensitivity highly depends on the type and brand of filament

For eel samples, it appears the environmental factor that appears to majorly contribute to the changes in measured resistance and therefore to each sample's sensitivity is humidity and not temperature. A pattern indicating that an increase in humidity results in a simultaneous increase in resistance and vice versa is observed in the cases of the 20%, 40%,60%,80% and 100% infill sample. For the single filament sample and the two samples with added protopasta layers, the changes in resistance values appear to be random and have no connection to humidity or temperature changes.

For pi-etu samples, the same pattern can be observed for samples with 40%,60%,80% and 100% infill. For every other case, the changes in sensor resistance are irrelevant to environmental factor changes and therefore random.

For filaflex samples, in almost every case, the changes in resistance that are measured are random. The only exception in the sample with 80% infill, which follows the same proposed pattern as the eel and pi-etu samples.

5. Discussion

5.1. Sensor design and data collection.

As mentioned in *Section 2.2.2*[(2.2.2)], it is crucial to secure the samples in place before each set of measurements. Since the resistance is measured in regard to pressure applied, in order to be able to compare the samples, when a certain weight is attached to the simulator the piston has to be aligned with the sample surface and remain so during the whole measurement process in order for the pressure applied to be uniform. Any change in the sample's position could result in a shift in the surface in contact with the piston and according to *Equation 4.1.4*, a change in the applied pressure.

Apart from securing the samples in the simulator, it is important to secure the connection between the sensor and the Arduino that measures the changes in resistance in order to avoid a short-circuit or a gap between the cables and the sensor that could affect the results. Experimentation has shown that using electrical paste, or a conductive glue in order to secure the circuit cables on the bottom and top of the sensor, results in a loss of all piezoresistive properties. The cables were eventually set on the two sides of the sensor with two pieces of non-conductive electrical tape, since this method not only did not compromise the piezoresistive properties of the sensor but allowed us to adjust the place of the cables before each measurement, therefore minimizing the possibility of a short-circuit caused by the wear of the surfaces due to the constant contact with the simulator.

After the data collection process is completed,a response diagram is created. (*Figure 2.3.1*, *Figure 2.3.2*) Ideally, the maximum and minimum peaks in the response diagrams should be in the form of plateaus instead of sharp peaks and have similar values, therefore signifying a consistency between the resistance values when both maximum and minimum pressure is applied. As shown in *Figure 5.1.1* and *Figure 5.1.2*, this is not always the case. The sharp points and the steep curves that appear instead of plateau especially in the case of the minimum values, have three potential causes. The first, is that the oscillation is not entirely harmonic. Therefore, the piston might bounce on the sensor causing peaks and drops in the measured resistance, especially when there is no weight attached to the simulator. Similarly, a smooth or rapid lift of the piston affects how the peaks corresponding to zero pressure applied, appear on the diagram. Furthermore, when any amount of pressure is applied, the sample being tested is deformed. When the pressure is lifted, it returns to its original state. How and how fast the sample returns to its original state cannot be measured since it changes with each oscillation, therefore differentiating each peak from all the others and thus contributing in the creation of the observed points and steep curves. Finally, experimentation with an ohmmeter connected to the sensors before they were placed on the gait simulator has shown that the initial sensor resistance, without pressure applied is not stable.

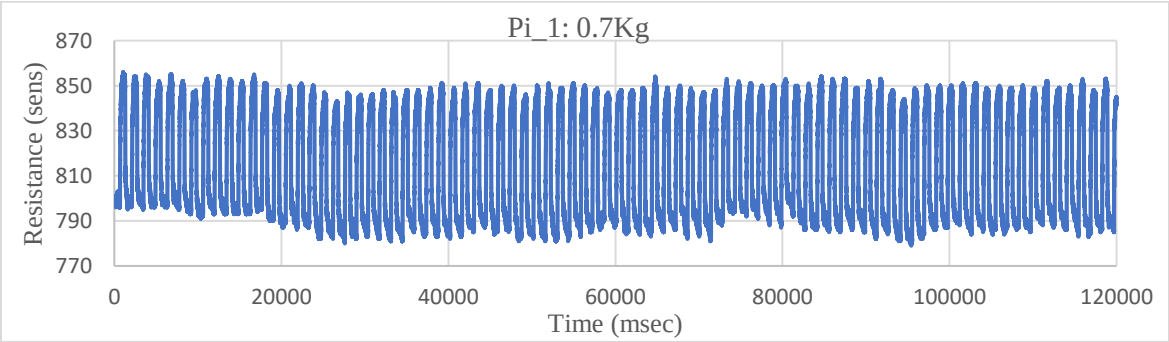

Figure 5.1.1: Indicative response diagram with non-uniform minimum peaks. The potential causes of the differentiation of the minimum resistance values measured are mentioned above.

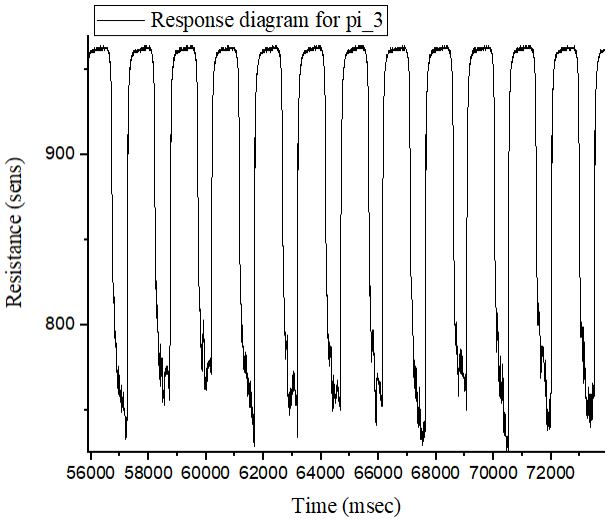

Figure 5.1.2: Indicative response diagram for pi_3 at 14.7Kg. The effect of the mentioned causes of differentiation on the minimum resistance values is obvious.

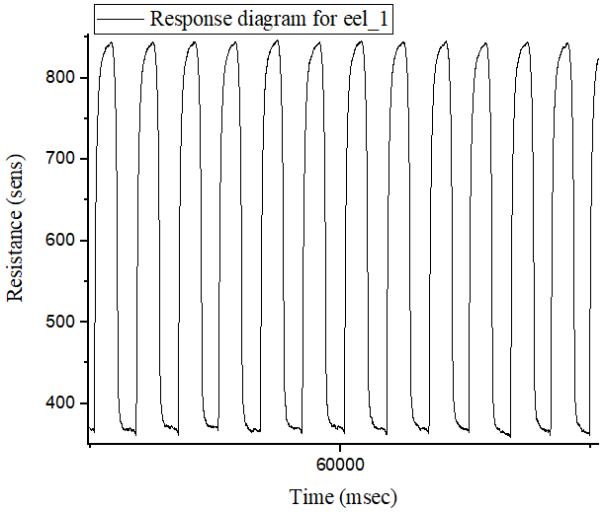

Figure 5.1.3: Indicative response diagram for eel_1 at 14.7Kg. The effects of the mentioned differentiation causes are not visible.

As proposed in *Figure 5.1.2* and *Figure 5.1.3*, it is not possible to predict how and if the error factors will affect each measurement. Therefore, in order to minimize the effect of these factors in the final results, the 10 maximum and minimum peaks that appear to be more uniform were chosen while the final Resistance-Pressure diagrams were created taking into consideration only the resistance values that correspond to the maximum peaks, as mentioned in *Section 3: Data Collection* [(3)].

Measurements for the aging tests included measuring the temperature and humidity percentage of the laboratory before each set of measurements. It is noted here that for the sensors printed in 2021, the validity of these measurements as can be observed in *Tables 3.1.1,3.1.2.,3.1.3* is uncertain and therefore were not included. An aspect that might affect the validity of humidity percentage and temperature measurements is the fact that the experiment was not concluded in ideal laboratory conditions but in a shared laboratory space in which the temperature and humidity could not be kept constant. Furthermore, during the measurement process, the sensors themselves were exposed to the changing temperature and humidity of the testing space, and regarding the samples printed in 2021 a flood in the laboratory.

5.2. Data analysis

5.2.1. Original measurements

In *Table 2.1.3.* both the single filament samples and the samples with 100% infill are mentioned. A closer observation will show that these samples have no structural differences and evidently both names describe the exact same sensor. The difference between them, and the reason that they are tested as different samples is the date of printing. The single filament samples have been printed and initially tested on $21/10/2021$, while the 100% infill ones, were initially tested on $08/02/2022$ (eel), $25/02/2022$ (pi-etu) and $11/03/2022$ (filaflex). Along with the fact that for every design a set of three samples was printed and tested, the simultaneous testing and comparison of sets of the same sensors printed with a gap of approximately four months between each print, prove that each print is different and even if the design, filament and printing factors are kept the same. Therefore, it is not possible to guarantee that the results associated with a certain sample will not change during further testing, thus indicating that the sensors tested in this study are not suitable for smart insole applications.

According to *Figure 4.2.25*, the steepest Resistance-Pressure curve, which indicates the highest sensitivity to pressure changes, belongs to the filaflex samples with a top and bottom protopasta layer. According to *Table 4.2.1*, these samples have the second smallest fast decay rate at $-49.30 \pm 5.14 MPa^{-1}$ while the single filament filaflex samples have a fast decay rate of -204.08 ± 400.00. It is observed though, that the decay

rate error for the single filament samples has an error that by far surpasses the value therefore indicating that the calculated decay rate does not correspond to reality. According to *Figure 4.2.24*, the resistance values that correspond to $(0.279 \pm 0.028)\,MPa$, and $(0.398 \pm 0.040)MPa$ seem to deviate from the fitting curve, indicating that the original measurements were corrupted. Furthermore, after changing the y axis scale from linear to Neper logarithmic the proposed one-phase exponential formula is not verified since two different slopes appear in the resulting diagrams, once again indicating that the measurements resulting in the one-phase exponential formula best describing the single filament eel samples and the eel samples with a 100% may also be a result of corrupted initial measurements. Apart from the environmental factors such as humidity and temperature that could not be kept entirely stable, as mentioned before major factors contributing in measurements that do not correspond to reality are the instability of the oscillation especially when small amounts of weight are attached to the oscillator and technical errors such as failure to properly align the tested sample with the simulator piston.

In *Figure 5.2.1*, the collective Resistance-Pressure diagram for all samples is shown. It is obvious, that the error bars that appear on the diagram hinder the identification of each curve, and seem to be significantly large compared to the values themselves. This is also observed in most of the diagrams shown in this thesis in which the values shown are not original measurements but average values of collected data. The reason behind this phenomenon is that the original measurement errors, are in many cases comparable to the values themselves since as previously mentioned the factors that contribute to error appearance are not possible to be transcended. Therefore, when the average of the measured resistance values is calculated, the corresponding errors calculated with error propagation formula, result to be also comparable to the average values and therefore resulting in the appearance of large error bars in the diagrams.

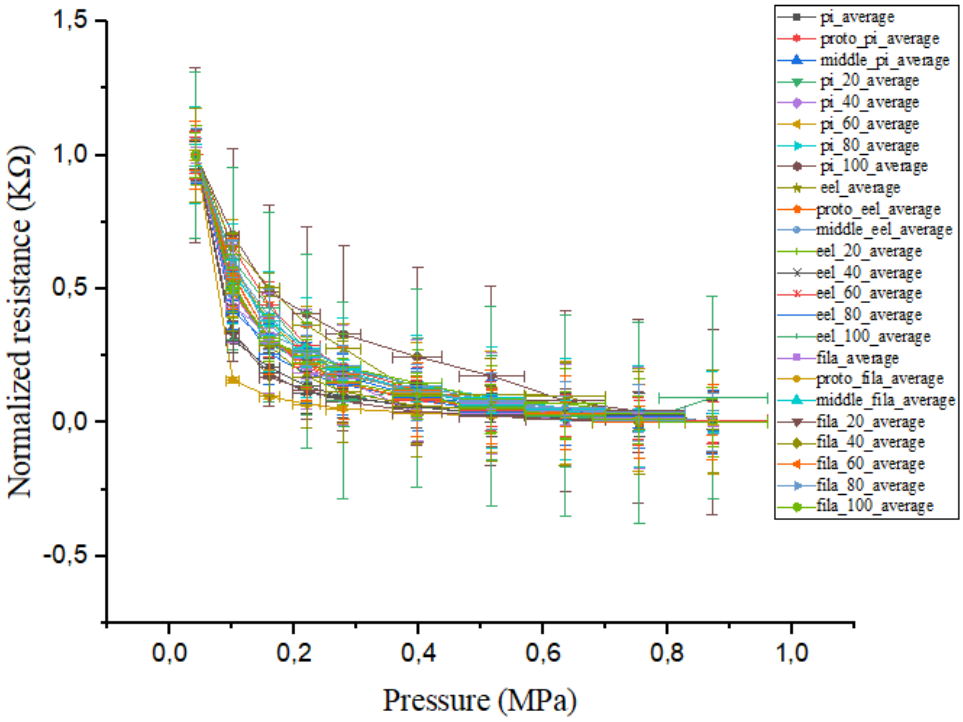

Figure 5.2.1: Collective Resistance-Pressure diagram with visible x,y error bars.

5.2.2.Aging

As previously mentioned, in order to measure how temperature and humidity affect sensor sensitivity, a pattern indicating how environmental changes affect measured resistance should be proposed. Although by close observation of the Resistance- Dates diagrams it seems that in most cases a pattern regarding the relationship between humidity and resistance does appear, individual deviations such as the one happening in

the case of the ell sample with 40% infill on 15/04 along with the fact that the proposed pattern is not consistent for both single filament samples and samples with 100% infill indicate that the possibility of the observed pattern being entirely coincidental is high.

In order to indicate if the proposed pattern is valid and the effect humidity and temperature have on the 3D printed sensors, further testing is necessary, since as previously mentioned, due to the fact that the laboratory where the experiment was concluded is shared, the temperature and humidity percentage could not be adjusted. Furthermore, in order to have a more objective view of how exposure to the laboratory environment and continued testing can affect sensitivity to pressure changes, the aging tests should be concluded with a greater number of measurements in order to eliminate individual technical errors.

5.3 Further Experimentation

The object of this study and the performance evaluations that were concluded was to examine if the piezoresistive properties of specific materials or sensor designs are sensitive enough to be utilized in smart insole applications. As proposed before, even minor alterations in a person's gait have significant diagnostic value, since they might reveal an undergoing medical condition thus the properties of the sensor element of a smart insole are of crucial importance.

In *Figure 5.3.1,* the system's architecture where the piezoresistive sensors were used is shown. The design, consists of the insole with the embedded sensors and a low-cost external system which due to its lightness and low power consumption is portable and is used to record and analyze the collected data in real time.

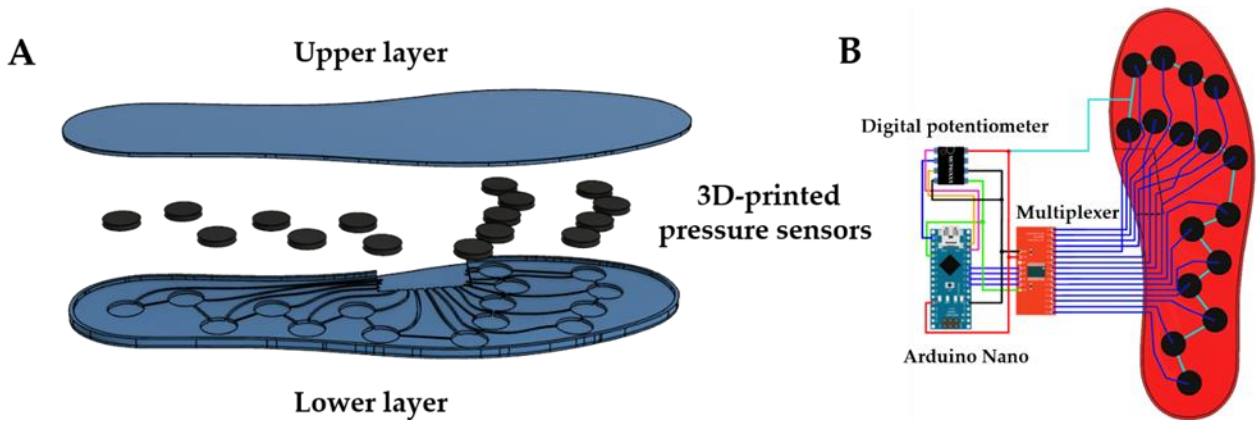

Figure 5.3.1: A) The 3D printed smart insole architecture. B) The circuit that connects the piezoresistive sensors inside the insole with the external data collector unit.

In *Figure 5.3.2* the pressure pattern that appears during the use of a 3D printed smart insole, which utilizes piezoresistive sensors is presented. It is clear how the pressure points change from the back to the front as the step progresses, but it appears that some of the sensors seem to be triggered even without pressure applied which raises the question of how such random resistance changes irrelevant to pressure application might affect the final results and how suitable piezoresistive sensors are for such applications. In comparison, in *Figure 5.3.3* the results of previous real time experiments with capacitive sensors are shown. It should be noted here that the sensitivity of the program used to record the pressure changes could be customized. Therefore, if the sensitivity of the program is high, which was the case for the piezoresistive sensors, it is more likely to reach the highest point in the chromatic scale, without the change in the sensor's resistance being major.

As therefore proposed before and in other works [31] further, more precise and targeted experimentation is necessary for the optimization of these types of sensors as current data indicates that they are less pressure-sensitive that the 3D printed capacitive ones.

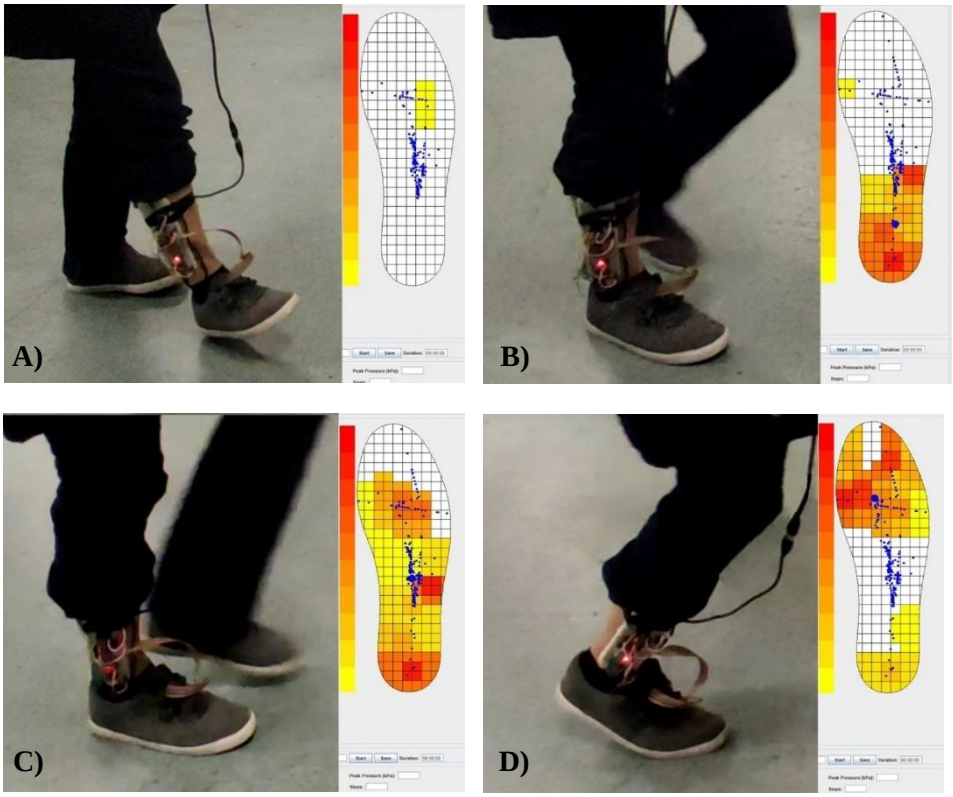

Figure 5.3.2: Testing of the 3D printed insole with piezoresistive sensors in real time (A, B, C, D).

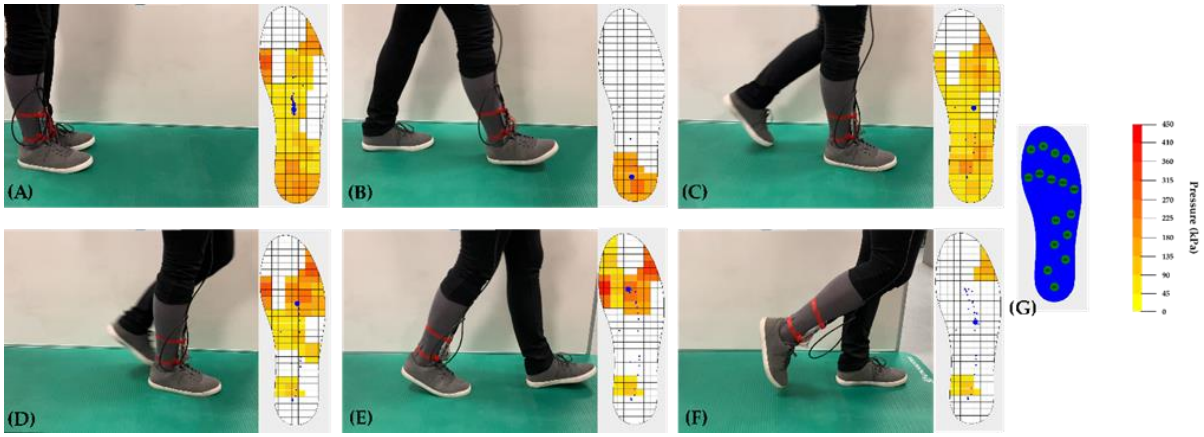

Figure 5.3.3: Testing of the 3D printed insole with capacitive sensors (A, B, C, D, E, F) in real time and sensor placement (G).

6. Conclusion

Taking into consideration the results presented and discussed in *Section 4: Data Analysis* and *Section 5: Discussion,* it is proposed that further experimentation and development is necessary in order to improve the sensitivity and response of the sensors, especially for high pressures in order to utilize 3D printed piezoresistive sensors, printed with a flexible filament are suitable in smart insoles.

As proposed in *Section 2: Materials and Methods,* flexible filaments in raw material form have a set volumetric resistivity proposed by the manufacturer. This volumetric resistivity is an indicator of each filament's conductivity but is not proportional to the final print's resistance which is affected by the printing temperature and velocity along with the structure and size of the design. Furthermore, the instability of each sensor's resistance even in a relaxed state which indicates that the measured resistance even for simultaneously printed sensor varies, proposes that it is almost impossible to propose a set value for the resistance of the sample when zero pressure is applied. Additionally, since the size of the sensors is required to be small, with a height and diameter of $3mm$ and $14.5mm$ respectively, noticing errors during the printing process that may result in further alteration of the printed sensor's sensitivity and piezoresistive properties, is a challenge.

The creation of a wearable smart insole for diagnostic purposes, requires the sensors placed inside to have a high pressure sensitivity in order to accurately monitor the wearer's gait cycle and the possible changes that may occur, but at the same time to be durable enough to withstand constant and rapid changes in pressure with minimum wear. Furthermore, the sensors should be unaffected by constant changes in humidity and temperature.

Continuous testing of the same samples on the simulator during this study has proven to be mildly destructive to each sample's surface, therefore indicating that the delicate nature of the sensors' design might compromise the obtained results. In addition to that, as previously stated, the sensors tested are proven to be highly affected by humidity and temperature changes, thus adding another factor to consider during monitoring the sensors inside a 3D printed insole. Therefore, distinguishing which changes in the measured resistance are caused by the sensor itself and its relation to pressure and environmental factors and which are an indicator of a differentiation in the gait cycle of the user will be a challenge.

Despite the proposed challenges, further experimentation in real time, with piezoresistive sensors placed inside a smart insole has shown that there are promising results in utilizing 3D printed sensors in smart insoles. Such gait analysis systems that track the wearers gait on real time can aid in the detection of changes in the gait cycle that might lead to the early prognosis of age-progressive neurological disorders such as Alzheimer's, Parkinson's, HIBM etc. Since treatment staring before such conditions progress can significantly increase the patient's quality of life the need for the development of portable and accessible diagnostic systems is imminent.

7. References

1. Kharb A. et all. (2011) 'A review of gait cycle and its parameters', *International Journal of Computational Engineering and Management,* vol.13
2. Samer M. et all, (2016) 'Recognition of gait cycle phases using wearable sensors', *Robotics and Autonomous Systems,* vol. 75(A), p.50-59, DOI:10.1016/j.robot.2014.10.
3. Borelli G.A. (1680) as cited in Baker R. (2007) 'The history of gait analysis before the advent of modern computers', *Gait & Posture,* vol. 26(3), p.331-342, DOI:10.1016/j.gaitpost.2006.10.014
4. Winter A.D. (1989) 'Biomechanics of Normal and Pathological Gait, Implications for Understanding Human Locomotor Control', *Journal of Motor Behavior,* vol.21(4), DOI: 10.1080/00222895.1989.10735488
5. Cappozzo A. (1984) 'Gait analysis methodology', *Human Movement Science,* vol. 3(1-2), p.27-50, DOI:10.1016/0167-9457(84)90004-6
6. Teckscan. "Gait Analysis Sustems" retrieved from: *https://www.tekscan.com/gait-analysis-systems*
7. BCN3D. 'When Was 3D Printing Invented? The History of 3D Printing', (2020) retrieved from: *https://www.bcn3d.com/the-history-of-3d-printing-when-was-3d-printing-invented/*
8. Wong K., Hernandez A. (2012) 'A review of additive manufacturing', *International Scholarly Research Network, vol.2012,* pages:10. DOI: 10.5402/2012/208760
9. Ahart M. (2019) 'Types of 3D printing technology' [Blog Post], retrieved from: *https://www.protolabs.com/resources/blog/types-of-3d-printing/*
10. Jacobs P. (1992), '*Rapid Prototyping and Manufacturing: Fundamentals of Stereolithography',* Valencia, California: Society of Manufacturing Engineers
11. O'Neil P. (2018) 'Internal void fabrication via mask projection micro-stereolithography: A rapid repeatable microfluidic prototyping technique', *Thesis for PhD Mechanical Engineering, Dublin City University,* DOI:10.13140/RG.2.2.14152.78080
12. Jones G. (2021) 'Direct Metal Laser Sintering (DMLS) – Simply Explained' *ALL3DP,* retrieved from:*https://all3dp.com/2/direct-metal-laser-sintering-dmls-simply-explained/*
13. Longhitano G. et all, (2015) 'Surface Finishes for Ti-6Al-4V Alloy Produced by Direct Metal Laser Sintering', *Materials Research,* vol.18(4), p. 838-842, DOI:10.1590/1516-1439.014415
14. Kampker A. et all, (2019), 'Review on Machine Designs of Material Extrusion based Additive Manufacturing (AM) Systems - Status-Quo and Potential Analysis for Future AM Systems', *Procedia CIRP, vol.89,* p. 815-819, DOI:10.1016/j.procir.2019.03.205
15. Murr L. (2012), 'Metal Fabrication by Additive Manufacturing Using Laser and Electron Beam Melting Technologies',*Journal of Materials Science & Technology,* vol.28(1), p.1-14. DOI: 10.1016/S1005-0302(12)60016-4
16. Grames E. (2020), 'What Is FDM 3D Printing? – Simply Explained', *ALL3DP,* retrieved from: *https://all3dp.com/2/fused-deposition-modeling-fdm-3d-printing-simply-explained/*
17. O'Connell J. (2020) 'The Types of FDM 3D Printers (Cartesian, CoreXY, & More)' *ALL3DP,* retrieved from: *https://all3dp.com/2/cartesian-3d-printer-delta-scara-belt-corexy-polar/*
18. Alex M. (2017) 'The 4 Types of FFF / FDM 3D Printer Explained (Cartesian, Delta, Polar)' *3DNatives,*retrieved from: *https://www.3dnatives.com/en/four-types-fdm-3d-printers140620174/#!*
19. Piezoresistive effect (2014), *Comsol Multiphysics Cyclopedia,* retrieved from: *https://www.comsol.com/multiphysics/piezoresistive-effect*
20. Piezoresistive effect, n.d., *Kistler,* retrieved from*: https://www.kistler.com/en/glossary/term/piezoresistive-effect/*
21. Chang L. (2012), '*Foundations of MEMS.*' (2nd Edition), Upper Saddle River, NJ: Pearson Education, Inc.

22. Barlian A.A. et all, (2009), ‘Review: Semiconductor Piezoresistance for Microsystems’, *Proc IEEE Inst Electr Electron Eng.* vol. 97(3): p.513–552. DOI: 10.1109/JPROC.2009.2013612.
23. Kim J. et all (2021), ‘Effects of 3D Printing-Line Directions for Stretchable Sensor Performances’, *Materials Special Issue: Experimental Testing and Numerical Simulation of Polymer-Based Additive Manufacturing Parts*n.p.s. DOI: 10.3390/ma14071791
24. Piezoresistive Pressure Sensors retrieved from: *https://www.avnet.com/wps/portal/abacus/solutions/technologies/sensors/pressure-sensors/core-technologies/piezoresistive-strain-gauge/*
25. Xu et all, (2017) ‘The boom in 3D-printed sensor technology’*SensorsSpecial Issue: Micro and Nanofabrication Technologies for Biosensors*vol.17(5), p.1166, DOI: 10.3390/s17051166
26. Laszczak P et all. (2015) ‘Development and validation of a 3D-printed interfacial stress sensor for prosthetic applications’, *Medical Engineering and Physics*, vol.37(1), p.132-137, DOI: 10.1016/j.medengphy.2014.10.002
27. Saari M. et all. (2016) ‘Fabrication and Analysis of a Composite 3D Printed Capacitive Force Sensor’. *3D Printing and Additive Manufacturing*, vol.3(3), p.136–141. DOI: 10.1089/3dp.2016.0021.
28. Suaste-Gómez E. et all, (2016),’Developing an Ear Prosthesis Fabricated in Polyvinylidene Fluoride by a 3D Printer with Sensory Intrinsic Properties of Pressure and Temperature.’,*Sensors(Basel)*, vol.16(3), p.332, DOI: 10.3390/s16030332
29. Lin Y.K. et all. (2016),’Using Three-Dimensional Printing Technology to Produce a Novel Optical Fiber Bragg Grating Pressure Sensor’. *Sensors and Materials*, vol.28(5) p.389–394. DOI: 10.18494/SAM.2016.1189
30. Md Omar Faruk Emon,Jae-Won Choi (2017),’Flexible Piezoresistive Sensors Embedded in 3D Printed Tires’ *Sensors(Basel)*, vol.17(3) p.656. DOI: 10.3390/s17030656.
31. Spinthaki S. (2021) “Ανάπτυξη 3D εκτυπωμένων χωρητικών αισθητήρων πίεσης για εφαρμογές σε ανάλυση βαδίσματος” [Bachelor’s dissertation, University of Crete]
32. Autodesk Inc. (2022), ‘Autodesk Fusion 360’, retrieved from: *https://www.autodesk.com/products/fusion-360/overview?term=1-YEAR&tab=subscription*
33. Drives F. (2018) ‘Eel 3D Printing Filament’ *Ninjatek*
34. Palmiga Innovation, (2016) ‘PI-ETPU 95-250 Carbon Black’ *Palmiga Innovation*
35. Recreus Industries S.L. (2018) ‘Conductive Filaflex’ *Recreus Industries S.L.*
36. ProtoPlant (2022) ‘Conductive PLA’, *ProtoPlant*
37. Prusa (2021)’3D Printing Handbbok: User manual for Original Prusa i3 MK3S+ Kit and Original Prusa i3 MK3S+’ *Prusa Research.*
38. Tenlog (2020) ‘Tenlog TL-D3 Pro User Manual’ *Shenzhen Tenlog 3D Technology co.*
39. Ultimaker BV., (2021) ‘UltimakerCura’, retrieved from: *https://ultimaker.com/software/ultimaker-cura*
40. Origin Pro, *Origin Lab*, retrieved from: https://www.originlab.com/

A. Measurement Appendix.

A.1. Single filament Eel sensors:

Max	eel_1		eel_2		eel_3	
Weight(kg)	Value	STDEV	Value	STDEV	Value	STDEV
0.7	588.00	1.41	453.40	2.24	693.30	3.16
1.7	704.40	0.92	549.70	6.04	750.00	5.85
2.7	751.20	1.54	619.90	11.44	771.00	1.58
3.7	789.50	1.75	669.20	6.44	816.70	3.72
4.7	806.30	2.10	738.00	4.67	824.10	3.65
6.7	834.00	1.34	877.40	1.02	863.80	18.68
8.7	841.30	1.19	886.10	0.94	859.40	2.65
10.7	838.00	1.18	892.00	0.89	859.30	1.49
12.7	844.30	1.55	890.20	1.08	936.60	4.05
14.7	845.10	0.94	895.50	0.81	936.60	1.28

Table A.1.1: Table of resistance values corresponding to the average of 10 max peaks, in regard of weight for single material eel sensors in fixed values.

Min	eel_1		eel_2		eel_3	
Weight(kg)	Value	STDEV	Value	STDEV	Value	STDEV
0.7	428.40	0.92	251.30	2.05	459.50	4.72
1.7	416.20	0.60	236.50	2.88	437.10	4.57
2.7	411.00	1.41	221.40	1.35	410.30	2.72
3.7	404.90	0.94	200.90	2.28	401.10	1.87
4.7	400.60	1.02	200.40	2.76	389.20	2.32
6.7	400.30	0.46	439.50	1.96	339.70	3.93
8.7	382.70	0.78	440.30	1.95	317.20	3.52
10.7	385.00	1.95	434.80	2.04	318.30	3.58
12.7	376.70	1.27	412.90	1.14	337.40	7.57
14.7	368.50	1.80	413.70	2.37	461.90	3.65

Table A.1.1: Table of resistance values corresponding to the average of 10 min peaks, in regard of weight for single material eel sensors in fixed values.

A.2. Eel sensors with top and bottom protopasta layers

Max	proto_eel_1		proto_eel _2		proto_eel _3	
Weight(kg)	Value	STDEV	Value	STDEV	Value	STDEV
0.7	829.90	0.99	747.10	1.97	764.40	0.97
1.7	884.70	0.67	849.70	1.64	838.30	1.06
2.7	902.00	1.49	884.50	1.72	872.20	1.99
3.7	915.80	0.63	896.20	1.14	890.80	1.40
4.7	924.10	2.02	907.80	0.92	899.80	1.40
6.7	933.60	0.52	919.90	0.74	910.80	0.79
8.7	939.40	0.52	929.50	0.97	922.40	0.84
10.7	945.60	0.52	937.20	1.23	933.90	0.88
12.7	948.40	0.52	942.00	0.82	938.40	0.70
14.7	950.50	0.71	943.40	0.70	942.20	0.79

Table A.2.1: Table of resistance values corresponding to the average of 10 max peaks, in regard of weight for eel sensors with two protopasta layers in fixed values.

Min	proto_eel _1		proto_eel _2		proto_eel _3	
Weight(kg)	Value	STDEV	Value	STDEV	Value	STDEV
0.7	696.60	1.07	496.90	1.66	517.00	1.33
1.7	690.30	1.16	474.80	3.29	475.50	2.27
2.7	690.10	2.60	474.60	1.96	459.40	1.51
3.7	690.30	1.95	461.50	2.51	439.70	2.11
4.7	678.60	2.72	459.10	2.51	425.60	1.96
6.7	698.40	2.22	439.80	2.39	420.60	2.01
8.7	720.30	2.26	456.60	1.71	427.60	1.90
10.7	712.10	1.66	455.40	2.50	431.30	1.95
12.7	721.80	3.12	450.70	2.31	417.70	2.67
14.7	699.90	2.33	460.40	3.72	447.10	2.42

Table A.2.2: Table of resistance values corresponding to the average of 10 min peaks, in regard of weight for eel sensors with two protopasta layers in fixed values.

A.3. Eel sensors with top, bottom and middle protopasta layers.

Max	middle_eel_1		middle_eel_2		middle_eel_3	
Weight(kg)	Value	STDEV	Value	STDEV	Value	STDEV
0.7	787.60	2.12	772.20	3.74	829.90	0.99
1.7	841.50	1.78	831.70	5.17	884.70	0.82
2.7	893.10	2.02	900.50	3.27	901.90	1.45
3.7	918.00	0.47	897.70	3.77	915.70	0.48
4.7	926.30	0.95	912.80	2.39	923.00	1.15
6.7	940.00	0.67	930.00	4.03	933.40	0.52
8.7	950.80	0.42	944.00	1.41	939.20	0.63
10.7	955.00	0.94	949.30	1.57	945.70	0.48
12.7	957.70	1.25	968.50	1.35	948.30	0.48
14.7	963.10	0.74	966.10	1.10	950.60	0.52

Table A.3.1: Table of resistance values corresponding to the average of 10 max peaks, in regard of weight for eel sensors with three Protopasta layers in fixed values.

Min	middle_eel_1		middle_eel_2		middle_eel_3	
Weight(kg)	Value	STDEV	Value	STDEV	Value	STDEV
0.7	478.40	6.17	652.60	3.37	696.60	1.07
1.7	482.70	3.77	642.90	4.15	688.90	1.20
2.7	461.70	2.26	567.30	3.83	690.20	1.40
3.7	433.60	6.47	614.30	4.47	690.90	1.91
4.7	409.90	5.59	579.00	7.23	679.20	2.97
6.7	434.40	3.84	538.33	4.61	697.80	2.30
8.7	434.40	3.84	563.30	4.03	718.90	2.18
10.7	464.60	3.66	600.30	5.23	712.10	1.73
12.7	436.90	2.96	603.10	4.46	722.10	3.14
14.7	496.10	6.94	635.50	1.72	700.30	2.79

Table A.3.2: Table of resistance values corresponding to the average of 10 min peaks, in regard of weight for eel sensors with three Protopasta layers in fixed values.

A.4. Eel sensors with 20% infill

Max 20%	eel_1		eel_2		eel_3	
Weight(kg)	Value	STDEV	Value	STDEV	Value	STDEV
0.7	746.00	2.83	595.60	4.29	643.40	4.13
1.7	816.50	1.57	703.90	2.70	763.40	2.80
2.7	871.30	1.19	768.10	3.27	800.50	1.57
3.7	884.00	1.55	776.00	2.41	825.50	3.20
4.7	892.20	1.40	790.60	2.11	837.80	4.28
6.7	914.40	0.92	809.30	2.33	851.50	1.96
8.7	923.10	0.94	819.40	2.01	888.60	2.29
10.7	931.00	0.89	815.30	3.49	899.40	1.43
12.7	936.30	1.49	845.70	1.35	901.70	1.27
14.7	940.90	1.76	857.10	2.62	918.10	2.26

Table A.4.1: Table of resistance values corresponding to the average of 10 max peaks, in regard of weight for 20% infill eel sensors in fixed values.

Min 20%	eel_1		eel_2		eel_3	
Weight(kg)	Value	STDEV	Value	STDEV	Value	STDEV
0.7	668.50	3.61	532.40	3.72	575.90	4.66
1.7	649.90	3.65	579.60	3.75	652.00	2.14
2.7	668.00	6.39	632.70	1.85	654.50	2.25
3.7	673.90	3.42	607.20	2.32	657.90	3.24
4.7	683.40	7.59	612.60	5.10	650.50	2.20
6.7	691.20	1.54	627.90	3.67	628.00	3.16
8.7	708.40	2.42	615.40	4.20	675.10	5.96
10.7	703.90	2.43	546.80	4.79	679.10	3.67
12.7	709.40	4.41	562.30	4.45	676.70	3.85
14.7	677.10	7.31	576.70	6.57	719.10	9.66

Table A.4.2: Table of resistance values corresponding to the average of 10 min peaks, in regard of weight for 20% infill eel sensors in fixed values

A.5. Eel sensors with 40% infill

Max	eel_1		eel_2		eel_3	
Weight(kg)	Value	STDEV	Value	STDEV	Value	STDEV
0.7	576.60	2.42	546.60	4.50	546.40	2.69
1.7	758.90	3.01	746.20	3.12	736.50	1.43
2.7	800.40	1.80	818.70	2.28	812.90	2.70
3.7	837.20	1.83	856.00	1.18	843.20	2.52
4.7	868.30	1.55	865.00	1.90	831.50	2.46
6.7	879.20	2.27	875.50	1.69	863.90	1.70
8.7	895.10	1.30	896.20	2.64	875.90	2.84
10.7	892.40	1.56	892.40	2.76	884.00	2.10
12.7	886.40	2.06	899.70	1.10	885.40	2.94
14.7	906.50	1.43	897.20	2.09	912.90	4.04

Table A.5.1: Table of resistance values corresponding to the average of 10 max peaks, in regard of weight for 40% infill eel sensors in fixed values.

Min	eel_1		eel_2		eel_3	
Weight(kg)	Value	STDEV	Value	STDEV	Value	STDEV
0.7	497.10	1.30	489.30	3.85	490.10	2.30
1.7	577.40	3.93	585.40	2.33	593.80	2.09
2.7	557.10	1.97	601.70	3.47	625.40	1.28
3.7	575.90	3.21	614.50	2.42	644.90	2.62
4.7	613.90	2.30	613.10	2.30	553.60	3.07
6.7	611.70	4.58	627.60	2.20	635.30	3.00
8.7	634.70	4.08	659.70	6.84	637.30	4.15
10.7	624.20	7.11	642.40	5.92	654.20	4.89
12.7	578.80	4.62	651.20	6.45	637.10	4.78
14.7	651.20	5.47	575.30	3.10	707.70	7.75

Table A.5.2: Table of resistance values corresponding to the average of 10 min peaks, in regard of weight for 40% infill eel sensors in fixed values.

A.6. Eel sensors with 60% infill

Max 60%	eel_1		eel_2		eel_3	
Weight(kg)	Value	STDEV	Value	STDEV	Value	STDEV
0.7	606.20	4.75	473.30	4.56	594.80	6.60
1.7	713.20	2.82	616.20	3.97	702.10	2.70
2.7	800.10	4.76	698.30	7.35	784.80	9.39
3.7	827.90	4.85	776.40	4.86	824.00	3.58
4.7	861.70	5.06	811.30	4.52	846.90	7.60
6.7	898.60	2.65	850.40	4.86	866.80	3.68
8.7	900.80	1.89	886.90	3.33	889.50	4.06
10.7	914.70	3.10	899.30	4.05	902.40	4.29
12.7	918.20	1.60	903.30	2.33	912.60	1.50
14.7	931.90	1.45	905.30	3.29	920.30	4.24

Table A.6.1: Table of resistance values corresponding to the average of 10 max peaks, in regard of weight for 60% infill eel sensors in fixed values

Min 60%	eel_1		eel_2		eel_3	
Weight(kg)	Value	STDEV	Value	STDEV	Value	STDEV
0.7	541.10	2.07	473.30	4.56	427.40	4.34
1.7	555.70	3.49	616.20	3.97	468.50	4.36
2.7	599.10	2.62	698.30	7.35	491.20	3.68
3.7	604.80	3.28	776.40	4.86	497.90	1.64
4.7	612.10	2.70	811.30	4.52	510.50	4.63
6.7	690.80	2.18	850.40	4.86	523.50	3.26
8.7	625.50	2.87	886.90	3.33	540.30	1.95
10.7	626.60	5.50	899.30	4.05	549.00	5.06
12.7	640.70	4.82	903.30	2.33	597.80	6.29
14.7	643.20	3.16	905.30	3.29	566.40	4.92

Table A.6.2: Table of resistance values corresponding to the average of 10 min peaks in regard of weight for 60% infill eel sensors in fixed values

A.7. Eel sensors with 80% infill

Max 80%	eel_1		eel_2		eel_3	
Weight(kg)	Value	STDEV	Value	STDEV	Value	STDEV
0.7	599.70	2.65	512.50	0.92	602.70	2.00
1.7	720.50	2.11	528.00	1.10	706.60	2.58
2.7	771.90	1.45	537.90	1.81	776.30	2.45
3.7	784.10	1.04	522.90	1.64	807.60	3.07
4.7	806.90	1.97	542.70	1.49	826.30	2.65
6.7	820.70	1.85	527.10	1.37	847.30	2.24
8.7	830.30	3.38	520.90	3.96	867.60	0.92
10.7	829.40	2.73	518.10	2.51	869.20	1.54
12.7	833.80	1.08	518.20	4.12	874.40	1.43
14.7	830.20	0.98	496.70	2.97	890.70	1.19

Table A.7.1:Table of resistance values corresponding to the average of 10 max peaks, in regard of weight for 80% infill eel sensors in fixed values

Min 80%	eel_1		eel_2		eel_3	
Weight(kg)	Value	STDEV	Value	STDEV	Value	STDEV
0.7	512.50	0.92	602.70	2.00	542.00	3.58
1.7	528.00	1.10	706.60	2.58	565.30	2.57
2.7	537.90	1.81	776.30	2.45	593.70	2.15
3.7	522.90	1.64	807.60	3.07	590.50	1.57
4.7	542.70	1.49	826.30	2.65	584.80	2.32
6.7	527.10	1.37	847.30	2.24	566.30	3.77
8.7	520.90	3.96	867.60	0.92	580.70	3.77
10.7	518.10	2.51	869.20	1.54	578.20	3.43
12.7	518.20	4.12	874.40	1.43	572.40	5.89
14.7	496.70	2.97	890.70	1.19	599.10	6.17

Table A.7.2:Table of resistance values corresponding to the average of 10 min peaks in regard of weight for 80% infill eel sensors in fixed values.

A.8. Eel sensors with 100% infill

Max	eel_1		eel_2		eel_3	
Weight(kg)	Value	STDEV	Value	STDEV	Value	STDEV
0.7	702.70	2.49	759.70	8.20	722.10	2.26
1.7	778.90	2.21	822.20	3.22	762.00	4.27
2.7	812.20	2.09	848.70	1.27	806.10	2.62
3.7	831.60	2.65	866.60	2.58	879.40	3.83
4.7	703.70	2.90	889.20	1.40	882.90	3.21
6.7	834.80	1.33	912.80	2.27	903.60	3.56
8.7	874.70	1.90	922.00	2.37	906.80	5.00
10.7	884.60	1.80	930.80	1.25	912.40	2.24
12.7	895.30	1.00	934.10	1.51	918.00	2.41
14.7	874.20	2.75	764.60	6.81	919.10	1.64

Table A.8.1:Table of resistance values corresponding to the average of 10 max peaks, in regard of weight for 100% infill eel sensors in fixed values

Min	eel_1		eel_2		eel_3	
Weight(kg)	Value	STDEV	Value	STDEV	Value	STDEV
0.7	649.50	4.43	712.70	2.49	605.70	1.79
1.7	681.80	1.08	727.20	3.31	556.00	5.46
2.7	678.80	1.78	733.00	2.97	503.50	3.32
3.7	674.90	3.24	736.10	2.66	598.75	3.69
4.7	647.00	3.55	743.80	1.83	536.20	7.26
6.7	683.80	2.18	769.30	3.52	550.70	3.58
8.7	672.00	3.97	773.80	3.99	545.50	3.53
10.7	683.10	2.39	799.20	4.85	679.90	7.12
12.7	715.80	3.46	794.40	2.76	651.20	8.36
14.7	605.10	3.94	712.60	2.46	647.60	6.05

Table A.8.2:Table of resistance values corresponding to the average of 10 min peaks in regard of weight for 100% infill eel sensors in fixed values

A.9. Single filament PI-ETU sensors

Max	pi_1		pi_2		pi_3	
Weight(kg)	Value	STDEV	Value	STDEV	Value	STDEV
0.7	852.80	1.72	849.20	1.40	860.70	2.00
1.7	882.50	0.67	903.50	1.02	903.10	1.04
2.7	908.60	0.49	930.70	0.90	917.00	0.89
3.7	923.80	0.40	948.90	0.54	932.10	0.54
4.7	934.80	0.40	954.90	0.30	943.60	0.66
6.7	948.00	0.00	962.90	0.30	949.40	0.49
8.7	955.10	0.30	970.10	0.30	954.20	0.40
10.7	964.00	0.00	971.20	0.40	957.50	0.50
12.7	970.50	0.50	973.00	0.00	959.90	0.30
14.7	976.00	0.00	960.60	0.49	964.00	0.00

Table A.9.1: Table of resistance values corresponding to the average of 10 max peaks, in regard of weight for single material pi sensors in fixed values

Min	pi_1		pi_2		pi_3	
Weight(kg)	Value	STDEV	Value	STDEV	Value	STDEV
0.7	752.6	1.7	785.3	1.6	751.3	2.5
1.7	757.6	1.4	792.0	1.3	794.6	1.5
2.7	758.4	3.2	798.8	2.2	818.1	1.9
3.7	769.1	2.8	809.1	1.4	827.2	1.7
4.7	775.2	2.2	811.5	3.0	837.7	1.7
6.7	783.3	2.2	806.5	3.1	604.4	4.3
8.7	770.0	3.1	835.6	3.4	630.2	14.2
10.7	791.9	2.5	816.1	3.5	651.5	3.3
12.7	787.9	2.0	827.3	1.3	680.9	3.8
14.7	791.2	2.1	781.9	2.9	760.9	3.9

Table A.9.2: Table of resistance values corresponding to the average of 10 min peaks, in regard of weight for single material pi sensors in fixed values.

A.10. Pi_ETU sensors with top and bottom protopasta layers

Max	proto_pi_1		proto_pi_2		proto_pi_3	
Weight(kg)	Value	STDEV	Value	STDEV	Value	STDEV
0.7	930.7	0.48	906.80	0.42	921.70	0.67
1.7	948.00	0.00	933.60	0.52	939.50	0.71
2.7	952.20	0.42	940.30	0.95	948.00	0.47
3.7	958.40	0.52	953.10	0.32	953.20	0.42
4.7	961.70	0.48	958.80	0.42	957.40	0.52
6.7	965.00	0.00	963.60	0.52	961.80	0.63
8.7	967.30	0.48	969.30	0.48	965.00	0.00
10.7	969.80	0.42	970.60	0.52	968.20	0.42
12.7	972.60	0.52	971.80	0.42	973.00	0.00
14.7	976.80	0.42	973.50	0.53	976.00	0.00

Table A.10.1: Table of resistance values corresponding to the average of 10 max peaks, in regard of weight for pi sensors with two protopasta layers in fixed values

Min	proto_pi_1		proto_pi_2		proto_pi_3	
Weight(kg)	Value	STDEV	Value	STDEV	Value	STDEV
0.7	858.10	1.29	841.50	0.97	778.00	2.40
1.7	842.20	1.03	823.40	0.97	740.40	3.72
2.7	816.80	2.39	754.90	4.72	694.90	2.08
3.7	814.10	1.66	794.60	1.78	655.10	3.96
4.7	819.80	1.32	747.10	2.69	660.20	3.16
6.7	818.50	2.64	735.30	2.67	677.90	2.85
8.7	818.30	1.57	766.50	5.93	686.60	4.30
10.7	833.20	1.62	769.40	2.41	728.00	4.22
12.7	836.30	1.77	771.60	7.32	751.50	3.54
14.7	821.90	1.73	807.60	2.32	755.10	4.51

Table A.10.2: Table of resistance values corresponding to the average of 10 min peaks, in regard of weight for pi sensors with two protopasta layers in fixed values.

A.11. Pi sensors with top, bottom and middle protopasta layers

Max	middle_pi_1		middle_pi_2		middle_pi_3	
Weight(kg)	Value	STDEV	Value	STDEV	Value	STDEV
0.7	761.30	1.77	732.10	3.96	804.70	3.83
1.7	858.10	1.20	870.40	3.53	881.60	2.27
2.7	876.80	1.23	898.70	1.57	913.00	1.33
3.7	892.60	1.07	918.50	1.27	913.20	1.48
4.7	909.50	1.08	925.50	2.37	931.50	1.18
6.7	931.00	1.15	948.60	1.35	942.50	1.18
8.7	929.50	0.85	966.80	0.42	948.10	1.52
10.7	934.40	1.78	966.20	0.92	956.70	1.06
12.7	942.40	0.52	971.60	0.52	968.00	0.67
14.7	950.50	1.43	976.30	0.48	965.20	0.63

Table A.11.1: Table of resistance values corresponding to the average of 10 max peaks, in regard of weight for pi sensors with three protopasta layers in fixed values.

Min	middle_pi_1		middle_pi_2		middle_pi_3	
Weight(kg)	Value	STDEV	Value	STDEV	Value	STDEV
0.7	472.80	1.32	548.10	1.45	513.00	2.91
1.7	516.60	1.35	550.30	2.26	536.20	3.36
2.7	488.90	2.23	536.00	4.16	538.60	4.90
3.7	490.40	0.84	538.80	4.02	539.70	4.30
4.7	498.20	2.20	537.50	3.92	538.10	3.31
6.7	520.50	2.92	577.33	5.70	562.10	3.93
8.7	512.80	3.79	646.40	4.20	558.30	4.50
10.7	518.90	6.66	619.00	4.37	583.20	18.49
12.7	530.40	2.27	648.90	3.78	628.60	3.86
14.7	526.00	2.40	713.70	4.47	595.00	4.52

Table A.11.2: Table of resistance values corresponding to the average of 10 min peaks, in regard of weight for pi sensors with three protopasta layers in fixed values.

A.12. Pi sensors with 20% infill

Max	pi_1		pi_2		pi_3	
Weight(kg)	Value	STDEV	Value	STDEV	Value	STDEV
0.7	877.00	0.45	808.80	0.60	815.90	1.64
1.7	945.70	0.46	847.50	0.67	887.00	2.28
2.7	965.90	0.30	857.50	0.81	927.40	1.20
3.7	976.00	0.00	869.60	0.66	937.80	1.08
4.7	982.30	0.46	872.30	0.78	944.00	1.00
6.7	990.00	0.00	890.30	1.00	953.00	0.63
8.7	998.00	0.00	920.90	0.54	964.00	0.45
10.7	997.70	0.64	912.60	0.80	975.40	2.91
12.7	1001.20	0.40	924.30	1.00	979.50	0.92
14.7	996.00	0.00	913.00	0.63	981.70	0.46

Table A.12.1: Table of resistance values corresponding to the average of 10 max peaks, in regard of weight for 20% infill pi sensors in fixed values.

Min	pi_1		pi_2		pi_3	
Weight(kg)	Value	STDEV	Value	STDEV	Value	STDEV
0.7	808.80	0.60	815.90	1.64	708.60	1.96
1.7	847.50	0.67	887.00	2.28	741.30	2.19
2.7	857.50	0.81	927.40	1.20	779.30	2.41
3.7	869.60	0.66	937.80	1.08	790.50	2.29
4.7	872.30	0.78	944.00	1.00	788.70	1.95
6.7	890.30	1.00	953.00	0.63	791.20	1.17
8.7	920.90	0.54	964.00	0.45	803.70	2.49
10.7	912.60	0.80	975.40	2.91	826.60	2.58
12.7	924.30	1.00	979.50	0.92	839.60	3.72
14.7	913.00	0.63	981.70	0.46	859.40	0.66

Table A.12.2: Table of resistance values corresponding to the average of 10 min peaks, in regard of weight for 20% infill pi sensors in fixed values.

A.13. Pi sensors with 40% infill

Max	pi_1		pi_2		pi_3	
Weight(kg)	Value	STDEV	Value	STDEV	Value	STDEV
0.7	839.00	1.83	758.90	1.37	759.67	0.82
1.7	909.30	0.64	802.50	1.02	850.60	1.80
2.7	941.50	0.81	832.20	0.87	881.20	0.98
3.7	945.40	0.92	790.80	1.72	896.60	0.80
4.7	959.20	0.40	807.40	0.66	902.70	1.79
6.7	968.40	0.66	827.60	1.28	916.40	0.66
8.7	978.10	0.94	848.20	1.99	929.80	0.87
10.7	984.90	0.30	872.40	6.23	939.60	0.80
12.7	986.40	0.49	869.20	1.25	941.40	0.66
14.7	989.20	0.60	891.30	1.42	947.80	1.17

Table A.13.1: Table of resistance values corresponding to the average of 10 max peaks, in regard of weight for 40% infill pi sensors in fixed values.

Min	pi_1		pi_2		pi_3	
Weight(kg)	Value	STDEV	Value	STDEV	Value	STDEV
0.7	758.90	1.37	759.67	0.82	692.10	1.04
1.7	802.50	1.02	850.60	1.80	698.30	1.19
2.7	832.20	0.87	881.20	0.98	703.00	0.77
3.7	790.80	1.72	896.60	0.80	695.00	1.10
4.7	807.40	0.66	902.70	1.79	698.70	1.00
6.7	827.60	1.28	916.40	0.66	698.20	1.40
8.7	848.20	1.99	929.80	0.87	727.90	2.26
10.7	872.40	6.23	939.60	0.80	733.60	1.50
12.7	869.20	1.25	941.40	0.66	755.10	2.66
14.7	891.30	1.42	947.80	1.17	770.00	2.68

Table A.13.2: Table of resistance values corresponding to the average of 10 min peaks, in regard of weight for 40% infill pi sensors in fixed values.

A.14. Pi sensors with 60% infill

Max	pi_1		pi_2		pi_3	
Weight(kg)	Value	STDEV	Value	STDEV	Value	STDEV
0.7	832.11	0.31	801.50	0.50	759.11	0.87
1.7	899.00	0.77	838.40	1.20	852.50	0.92
2.7	923.80	0.60	843.70	0.46	890.90	1.22
3.7	941.90	0.94	853.80	0.98	914.80	0.75
4.7	954.50	1.12	860.90	1.87	929.00	0.63
6.7	966.00	0.67	867.30	1.55	942.60	0.66
8.7	974.30	0.64	882.70	1.27	948.70	1.00
10.7	979.50	0.50	880.00	1.41	951.80	1.66
12.7	982.20	0.60	886.10	0.94	959.10	0.30
14.7	984.70	0.64	894.40	1.85	960.40	1.36

Table A.14.1: Table of resistance values corresponding to the average of 10 max peaks, in regard of weight for 60% infill pi sensors in fixed values.

Min	pi_1		pi_2		pi_3	
Weight(kg)	Value	STDEV	Value	STDEV	Value	STDEV
0.7	801.50	0.50	759.11	0.87	712.20	0.87
1.7	838.40	1.20	852.50	0.92	748.80	0.98
2.7	843.70	0.46	890.90	1.22	759.40	1.20
3.7	853.80	0.98	914.80	0.75	778.00	0.89
4.7	860.90	1.87	929.00	0.63	802.10	1.14
6.7	867.30	1.55	942.60	0.66	799.80	1.17
8.7	882.70	1.27	948.70	1.00	810.50	1.36
10.7	880.00	1.41	951.80	1.66	818.00	2.10
12.7	886.10	0.94	959.10	0.30	828.10	2.12
14.7	894.40	1.85	960.40	1.36	831.30	1.73

Table A.14.2: Table of resistance values corresponding to the average of 10 min peaks, in regard of weight for 60% infill pi sensors in fixed values.

A.15. Pi sensors with 80% infill

Max	pi_1		pi_2		pi_3	
Weight(kg)	Value	STDEV	Value	STDEV	Value	STDEV
0.7	791.22	1.23	759.10	1.70	739.56	1.17
1.7	865.80	0.60	777.10	0.70	825.30	3.38
2.7	892.80	0.40	783.70	0.64	863.30	0.78
3.7	908.40	0.49	794.30	0.90	879.00	0.89
4.7	924.00	0.00	815.20	1.40	895.70	0.78
6.7	936.00	0.00	816.40	1.43	909.44	0.68
8.7	944.60	0.49	823.30	0.78	920.30	0.64
10.7	952.70	0.46	843.40	1.20	930.30	0.78
12.7	962.00	0.00	846.70	0.78	934.20	0.60
14.7	967.00	0.00	862.60	2.33	940.10	0.30

Table A.15.1: Table of resistance values corresponding to the average of 10 max peaks, in regard of weight for 80% infill pi sensors in fixed values.

Min	pi_1		pi_2		pi_3	
Weight(kg)	Value	STDEV	Value	STDEV	Value	STDEV
0.7	759.10	1.70	739.56	1.17	690.90	0.70
1.7	777.10	0.70	825.30	3.38	707.90	0.70
2.7	783.70	0.64	863.30	0.78	732.10	1.22
3.7	794.30	0.90	879.00	0.89	731.30	0.64
4.7	815.20	1.40	895.70	0.78	733.20	0.40
6.7	816.40	1.43	909.44	0.68	746.30	1.62
8.7	823.30	0.78	920.30	0.64	766.00	1.34
10.7	843.40	1.20	930.30	0.78	767.80	1.78
12.7	846.70	0.78	934.20	0.60	776.30	2.10
14.7	862.60	2.33	940.10	0.30	784.90	2.30

Table A.15.2: Table of resistance values corresponding to the average of 10 min peaks, in regard of weight for 80% infill pi sensors in fixed values.

A.16. Pi sensors with 100% infill

Max	pi_1		pi_2		pi_3	
Weight(kg)	Value	STDEV	Value	STDEV	Value	STDEV
0.7	873.00	0.00	865.00	0.00	895.00	0.00
1.7	891.90	0.30	875.00	0.00	927.10	0.30
2.7	917.70	0.46	899.00	0.00	945.00	0.00
3.7	923.80	0.40	903.00	0.00	952.50	0.50
4.7	933.00	0.00	910.00	0.00	961.10	0.30
6.7	945.56	0.50	919.20	0.40	965.00	0.00
8.7	954.20	0.40	926.40	0.49	970.33	0.47
10.7	968.60	0.49	937.70	0.64	979.00	0.00
12.7	971.10	0.30	939.20	0.40	984.30	0.46
14.7	977.80	0.40	941.40	0.66	987.00	0.00

Table A.16.1: Table of resistance values corresponding to the average of 10 max peaks, in regard of weight for 100% infill pi sensors in fixed values.

Min	pi_1		pi_2		pi_3	
Weight(kg)	Value	STDEV	Value	STDEV	Value	STDEV
0.7	865.00	0.00	895.00	0.00	885.50	0.00
1.7	875.00	0.00	927.10	0.30	899.80	0.40
2.7	899.00	0.00	945.00	0.00	912.80	0.00
3.7	903.00	0.00	952.50	0.50	919.80	0.40
4.7	910.00	0.00	961.10	0.30	927.50	0.50
6.7	919.20	0.40	965.00	0.00	926.40	0.49
8.7	926.40	0.49	970.33	0.47	930.30	0.46
10.7	937.70	0.64	979.00	0.00	940.40	0.49
12.7	939.20	0.40	984.30	0.46	948.00	0.00
14.7	941.40	0.66	987.00	0.00	954.00	0.00

Table A.16.2: Table of resistance values corresponding to the average of 10 min peaks, in regard of weight for 100% infill pi sensors in fixed values.

A.17. Single filament filaflex sensors

Max	fila_1		fila_2		fila_3	
Weight(kg)	Value	STDEV	Value	STDEV	Value	STDEV
0.7	542.40	3.07	683.40	2.58	751.60	1.80
1.7	720.00	2.05	786.40	2.33	867.90	1.30
2.7	726.50	1.36	832.50	1.12	902.90	1.70
3.7	834.80	1.54	848.70	1.27	933.10	0.83
4.7	808.40	1.28	877.20	1.78	942.00	0.45
6.7	901.70	0.46	922.00	0.45	950.10	0.30
8.7	909.70	0.78	930.00	0.45	935.70	0.46
10.7	926.50	0.92	935.90	0.30	942.60	0.49
12.7	931.70	0.64	925.70	0.64	943.90	0.54
14.7	928.00	1.00	941.70	0.46	945.90	0.70

Table A.17.1:Table of resistance values corresponding to the average of 10 max peaks, in regard of weight for single material filaflex sensors in fixed values.

Min	fila_1		fila_2		fila_3	
Weight(kg)	Value	STDEV	Value	STDEV	Value	STDEV
0.7	260.70	4.12	440.00	3.82	515.50	3.85
1.7	215.00	3.55	400.60	7.05	514.70	3.95
2.7	131.40	2.94	385.20	2.56	509.20	5.65
3.7	199.30	2.24	190.60	2.33	528.10	3.78
4.7	167.70	1.68	359.40	4.08	511.60	3.47
6.7	330.90	4.25	575.10	3.45	547.30	3.26
8.7	346.60	7.00	571.90	3.27	445.70	2.45
10.7	371.00	2.65	584.00	2.28	476.90	2.17
12.7	368.10	3.62	195.90	4.89	483.10	1.87
14.7	325.50	2.91	526.60	1.96	469.10	1.14

Table A.17.2:Table of resistance values corresponding to the average of 10 min peaks, in regard of weight for single material filaflex sensors in fixed values.

A.18. Filaflex sensors with top and bottom protopasta layers

Max	proto_fila_1		proto_fila _2		proto_fila _3	
Weight(kg)	Value	STDEV	Value	STDEV	Value	STDEV
0.7	879.80	0.79	796.20	1.23	778.70	2.36
1.7	906.50	1.35	852.50	1.18	906.40	1.17
2.7	922.20	1.03	888.90	0.88	941.20	1.40
3.7	932.60	0.70	905.00	1.05	955.50	0.97
4.7	938.30	0.48	925.10	0.74	952.30	0.82
6.7	945.30	0.48	931.00	0.67	966.00	0.47
8.7	949.80	0.42	940.50	0.53	969.00	0.00
10.7	954.40	0.52	930.90	0.57	972.50	0.53
12.7	956.90	0.32	950.00	0.47	975.70	0.48
14.7	960.00	0.00	958.20	0.42	980.80	0.42

Table A.18.1: Table of resistance values corresponding to the average of 10 max peaks, in regard of weight for filaflex sensors with two protopasta layers in fixed values.

Min	proto_fila _1		proto_fila _2		proto_fila _3	
Weight(kg)	Value	STDEV	Value	STDEV	Value	STDEV
0.7	724.30	1.95	657.30	1.77	518.10	2.02
1.7	694.20	1.69	617.30	1.89	540.30	2.36
2.7	679.60	0.70	604.20	2.74	566.90	7.80
3.7	681.70	1.16	605.30	3.47	577.10	5.80
4.7	683.10	1.45	583.20	2.39	546.80	3.88
6.7	689.30	2.41	611.30	2.50	635.00	4.11
8.7	675.90	1.29	600.50	2.07	648.60	8.38
10.7	682.40	1.96	612.10	2.51	663.70	2.11
12.7	686.10	4.53	584.60	2.76	693.80	2.94
14.7	689.40	3.31	596.90	3.35	723.20	2.94

Table A.18.2:Table of resistance values corresponding to the average of 10 min peaks, in regard of weight for filaflex sensors with two protopasta layers in fixed values.

A.19. Filaflex sensors with top, bottom and middle protopasta layers

Max	middle_fila_1		middle_fila_2		middle_fila_3	
Weight(kg)	Value	STDEV	Value	STDEV	Value	STDEV
0.7	806.80	1.48	844.20	0.42	782.90	1.79
1.7	869.70	1.06	894.20	0.42	844.60	2.72
2.7	886.80	1.03	906.90	0.74	886.20	1.75
3.7	904.70	0.95	920.70	0.48	908.20	2.15
4.7	914.90	0.74	929.00	0.00	916.10	1.66
6.7	930.20	2.04	936.30	0.48	931.90	1.52
8.7	936.20	1.23	942.80	0.42	941.00	1.76
10.7	942.50	0.53	944.50	0.71	945.80	2.20
12.7	942.70	1.16	950.20	0.42	954.20	2.04
14.7	948.90	0.57	952.00	0.82	954.20	1.03

Table A.19.1:Table of resistance values corresponding to the average of 10 max peaks, in regard of weight for filaflex sensors with three protopasta layers in fixed values.

Min	middle_fila_1		middle_fila_2		middle_fila_3	
Weight(kg)	Value	STDEV	Value	STDEV	Value	STDEV
0.7	686.7	1.4	777.8	0.4	593.4	2.8
1.7	661.3	0.7	771.5	0.5	545.2	2.9
2.7	592.4	1.2	687.1	1.2	569.9	4.4
3.7	582.2	3.3	708.9	2.0	550.0	2.6
4.7	554.9	0.7	716.2	1.6	539.1	6.3
6.7	487.7	3.7	712.8	3.0	549.0	4.2
8.7	474.1	6.4	710.6	5.0	525.2	7.6
10.7	529.3	2.2	719.6	2.4	510.2	3.6
12.7	499.4	2.9	738.5	3.0	549.5	4.0
14.7	510.3	3.9	750.3	2.5	603.1	4.6

Table A.19.2:Table of resistance values corresponding to the average of 10 min peaks, in regard of weight for filaflex sensors with three protopasta layers in fixed values

A.20. Filaflex sensors with 20% infil

Max	fila_1		fila_2		fila_3	
Weight(kg)	Value	STDEV	Value	STDEV	Value	STDEV
0.7	711.10	1.22	493.70	2.45	662.60	1.20
1.7	870.00	1.00	570.50	4.39	822.20	1.54
2.7	919.40	0.49	594.60	3.64	872.10	1.30
3.7	938.60	1.11	628.00	3.26	882.30	1.35
4.7	952.70	0.78	662.20	2.60	897.70	1.00
6.7	965.00	0.45	672.40	6.83	913.90	0.30
8.7	971.30	0.64	702.20	5.60	921.00	0.63
10.7	976.00	0.00	711.40	8.81	924.80	0.75
12.7	979.30	0.46	718.70	2.28	928.20	0.40
14.7	979.80	0.40	692.70	6.45	929.30	0.90

Table A.20.1:Table of resistance values corresponding to the average of 10 max peaks, in regard of weight for 20% infill filaflex sensors in fixed values.

Min	fila_1		fila_2		fila_3	
Weight(kg)	Value	STDEV	Value	STDEV	Value	STDEV
0.7	493.70	2.45	662.60	1.20	406.10	2.98
1.7	570.50	4.39	822.20	1.54	503.60	2.15
2.7	594.60	3.64	872.10	1.30	527.30	5.10
3.7	628.00	3.26	882.30	1.35	494.90	4.85
4.7	662.20	2.60	897.70	1.00	482.80	3.54
6.7	672.40	6.83	913.90	0.30	520.70	3.82
8.7	702.20	5.60	921.00	0.63	542.10	7.44
10.7	711.40	8.81	924.80	0.75	517.10	2.30
12.7	718.70	2.28	928.20	0.40	546.00	4.84
14.7	692.70	6.45	929.30	0.90	528.10	5.36

Table A.20.2:Table of resistance values corresponding to the average of 10 min peaks, in regard of weight for 20% infill filaflex sensors in fixed values.

A.21. Filaflex sensors with 40% infill

Max	fila_1		fila_2		fila_3	
Weight(kg)	Value	STDEV	Value	STDEV	Value	STDEV
0.7	787.80	0.87	746.50	0.67	775.70	1.00
1.7	866.20	1.47	789.50	2.25	836.10	0.70
2.7	915.70	1.19	806.70	1.49	867.60	0.92
3.7	936.80	1.17	805.60	2.01	899.60	0.80
4.7	951.70	1.00	815.70	1.49	908.00	0.63
6.7	962.70	0.46	820.70	2.33	922.20	0.75
8.7	964.70	0.64	818.70	1.49	926.60	0.49
10.7	969.10	0.54	828.30	1.90	930.50	0.50
12.7	976.00	0.00	842.20	1.17	936.00	0.00
14.7	976.00	3.00	843.90	2.84	935.60	0.49

Table A.21.1: Table of resistance values corresponding to the average of 10 max peaks, in regard of weight for 40% infill filaflex sensors in fixed values.

Min	fila_1		fila_2		fila_3	
Weight(kg)	Value	STDEV	Value	STDEV	Value	STDEV
0.7	746.50	0.67	775.70	1.00	711.10	0.54
1.7	789.50	2.25	836.10	0.70	742.40	5.94
2.7	806.70	1.49	867.60	0.92	738.40	0.49
3.7	805.60	2.01	899.60	0.80	738.80	0.40
4.7	815.70	1.49	908.00	0.63	734.90	0.94
6.7	820.70	2.33	922.20	0.75	747.40	0.80
8.7	818.70	1.49	926.60	0.49	753.70	3.20
10.7	828.30	1.90	930.50	0.50	758.60	1.50
12.7	842.20	1.17	936.00	0.00	764.70	1.19
14.7	843.90	2.84	935.60	0.49	764.90	2.39

Table A.21.2:Table of resistance values corresponding to the average of 10 min peaks, in regard of weight for 40% infill filaflex sensors in fixed values.

A.22. Filaflex sensors with 60% infill

Max	fila_1		fila_2		fila_3	
Weight(kg)	Value	STDEV	Value	STDEV	Value	STDEV
0.7	769.70	1.35	717.70	0.90	717.40	0.80
1.7	848.60	1.69	764.90	0.83	788.10	1.58
2.7	896.70	1.10	787.90	1.45	853.30	0.90
3.7	923.00	1.26	787.90	1.14	878.70	1.19
4.7	942.10	1.04	789.10	1.45	899.10	1.22
6.7	957.50	1.12	782.90	2.34	913.90	1.04
8.7	964.70	0.46	775.40	2.15	925.90	0.70
10.7	972.30	0.64	787.90	2.30	928.20	0.60
12.7	986.20	0.40	814.20	1.08	935.50	0.50
14.7	988.10	0.30	826.80	0.98	935.60	0.49

Table A.22.1: Table of resistance values corresponding to the average of 10 max peaks, in regard of weight for 60% infill filaflex sensors in fixed values.

Min	fila_1		fila_2		fila_3	
Weight(kg)	Value	STDEV	Value	STDEV	Value	STDEV
0.7	717.70	0.90	717.40	0.80	663.10	0.94
1.7	764.90	0.83	788.10	1.58	676.60	0.80
2.7	787.90	1.45	853.30	0.90	701.10	1.22
3.7	787.90	1.14	878.70	1.19	702.30	1.68
4.7	789.10	1.45	899.10	1.22	709.70	2.72
6.7	782.90	2.34	913.90	1.04	698.00	1.00
8.7	775.40	2.15	925.90	0.70	706.30	2.72
10.7	787.90	2.30	928.20	0.60	700.10	2.07
12.7	814.20	1.08	935.50	0.50	710.60	1.50
14.7	826.80	0.98	935.60	0.49	713.80	1.99

Table A.22.2: Table of resistance values corresponding to the average of 10 min peaks, in regard of weight for 60% infill filaflex sensors in fixed values.

A.23. Filaflex sensors with 80% infill

Max	fila_1		fila_2		fila_3	
Weight(kg)	Value	STDEV	Value	STDEV	Value	STDEV
0.7	642.40	1.11	601.90	1.30	684.20	1.66
1.7	755.30	2.90	638.20	2.60	757.80	1.54
2.7	807.50	1.50	632.00	1.79	801.30	2.33
3.7	845.60	0.66	640.90	2.30	844.30	1.68
4.7	872.60	1.11	652.80	1.60	877.00	2.00
6.7	901.00	1.00	661.00	1.41	899.30	1.27
8.7	916.10	0.94	673.70	1.62	916.00	0.63
10.7	931.90	1.58	684.50	3.14	927.40	0.49
12.7	931.90	1.58	684.50	3.14	936.80	0.87
14.7	952.50	0.81	698.60	2.29	954.00	0.00

Table A.23.1: Table of resistance values corresponding to the average of 10 max peaks, in regard of weight for 80% infill filaflex sensors in fixed values.

Min	fila_1		fila_2		fila_3	
Weight(kg)	Value	STDEV	Value	STDEV	Value	STDEV
0.7	601.90	1.30	684.20	1.66	649.10	0.94
1.7	638.20	2.60	757.80	1.54	662.50	2.06
2.7	632.00	1.79	801.30	2.33	655.40	1.62
3.7	640.90	2.30	844.30	1.68	659.00	1.61
4.7	652.80	1.60	877.00	2.00	678.40	2.20
6.7	661.00	1.41	899.30	1.27	682.10	1.81
8.7	673.70	1.62	916.00	0.63	689.70	1.90
10.7	684.50	3.14	927.40	0.49	689.40	1.28
12.7	684.50	3.14	936.80	0.87	685.00	2.32
14.7	698.60	2.29	954.00	0.00	554.20	2.40

Table A.23.2: Table of resistance values corresponding to the average of 10 min peaks, in regard of weight for 80% infill filaflex sensors in fixed values.

A.24. Filaflex sensors with 100% infill

Max	fila_1		fila_2		fila_3	
Weight(kg)	Value	STDEV	Value	STDEV	Value	STDEV
0.7	668.10	1.51	618.40	1.36	657.10	1.30
1.7	789.60	2.20	675.30	2.90	777.80	1.25
2.7	851.30	0.90	683.00	3.52	844.20	1.17
3.7	879.10	1.30	671.70	3.20	880.70	0.90
4.7	911.40	1.56	654.80	2.27	893.80	1.17
6.7	934.60	1.28	644.30	2.53	918.00	0.00
8.7	954.50	0.67	663.90	3.05	941.10	0.30
10.7	967.90	0.70	676.10	5.45	950.50	0.50
12.7	978.80	0.40	702.40	3.41	955.20	0.40
14.7	980.90	0.30	694.20	2.56	964.00	0.00

Table A.24.1: Table of resistance values corresponding to the average of 10 max peaks, in regard of weight for 100% infill filaflex sensors in fixed values.

Min	fila_1		fila_2		fila_3	
Weight(kg)	Value	STDEV	Value	STDEV	Value	STDEV
0.7	618.40	1.36	657.10	1.30	603.00	0.77
1.7	675.30	2.90	777.80	1.25	665.20	1.78
2.7	683.00	3.52	844.20	1.17	700.40	1.28
3.7	671.70	3.20	880.70	0.90	696.10	1.37
4.7	654.80	2.27	893.80	1.17	685.40	2.33
6.7	644.30	2.53	918.00	0.00	677.70	3.35
8.7	663.90	3.05	941.10	0.30	694.80	2.04
10.7	676.10	5.45	950.50	0.50	711.00	2.37
12.7	702.40	3.41	955.20	0.40	722.20	2.09
14.7	694.20	2.56	964.00	0.00	756.00	1.67

Table A.24.2: Table of resistance values corresponding to the average of 10 min peaks, in regard of weight for 100% infill filaflex sensors in fixed values.